NAVAL POSTGRADUATE SCHOOL

MONTEREY, CALIFORNIA

THESIS

NUMERICAL MODELING OF THE VERTICAL HEAT TRANSPORT THROUGH THE DIFFUSIVE LAYER OF THE ARCTIC OCEAN

by

Angela S. Lefler

March 2013

Thesis Advisor: Timour Radko
Second Reader: Jason Flanagan

Approved for public release; distribution is unlimited

THIS PAGE INTENTIONALLY LEFT BLANK

REPORT DOCUMENTATION PAGE	Form Approved OMB No. 0704-0188

1. AGENCY USE ONLY *(Leave blank)*	2. REPORT DATE	3. REPORT TYPE AND DATES COVERED
	March 2013	Master's Thesis

4. TITLE AND SUBTITLE
NUMERICAL MODELING OF THE VERTICAL HEAT TRANSPORT THROUGH THE DIFFUSIVE LAYER OF THE ARCTIC OCEAN

5. FUNDING NUMBERS

6. AUTHOR(S) Angela S. Lefler

7. PERFORMING ORGANIZATION NAME(S) AND ADDRESS(ES)
Naval Postgraduate School
Monterey, CA 93943-5000

8. PERFORMING ORGANIZATION REPORT NUMBER

9. SPONSORING /MONITORING AGENCY NAME(S) AND ADDRESS(ES)
N/A

10. SPONSORING/MONITORING AGENCY REPORT NUMBER

11. SUPPLEMENTARY NOTES The views expressed in this thesis are those of the author and do not reflect the official policy or position of the Department of Defense or the U.S. Government. IRB Protocol number ____N/A____.

12a. DISTRIBUTION / AVAILABILITY STATEMENT
Approved for public release; distribution is unlimited

12b. DISTRIBUTION CODE

13. ABSTRACT (maximum 200 words)
The Arctic Ocean has been a subject of increasing interest in recent years due to the reduction of the sea-ice thickness and spatial coverage and its implications for climate change. The future state of the Arctic is likely to be linked to vertical heat transport by microscale processes, specifically, double-diffusive convection. A series of realistic three-dimensional direct numerical simulations (DNS) were conducted to assess the vertical heat transport through thermohaline staircases in the Arctic region. Results revealed that vertical fluxes exceeded those of extant "four-thirds flux laws" by as much as a factor of two, and suggest that the 4/3 exponent requires downward revision. Results also showed that two-dimensional DNS can provide an accurate approximation of heat fluxes when the density ratio is sufficiently large. DNS results also reveal that the models with rigid boundaries result in heat flux estimates that are lower than those from models with periodic boundary conditions. Finally, the DNS-derived flux law was applied to Arctic data and results supported the conclusion that lab-derived flux laws significantly underestimate heat flux. All of these results suggest that vertical heat transport due to double-diffusive convection is a significant contributor to the measured reduction of Arctic sea-ice.

14. SUBJECT TERMS Double Diffusion, diffusive convection, Direct Arctic Ocean, double-diffusion, diffusive convection, flux law, numerical simulations, vertical heat flux, thermohaline staircase

15. NUMBER OF PAGES 73

16. PRICE CODE

17. SECURITY CLASSIFICATION OF REPORT	18. SECURITY CLASSIFICATION OF THIS PAGE	19. SECURITY CLASSIFICATION OF ABSTRACT	20. LIMITATION OF ABSTRACT
Unclassified	Unclassified	Unclassified	UU

NSN 7540-01-280-5500 Standard Form 298 (Rev. 2-89)
Prescribed by ANSI Std. 239-18

THIS PAGE INTENTIONALLY LEFT BLANK

Approved for public release; distribution is unlimited

NUMERICAL MODELING OF THE VERTICAL HEAT TRANSPORT THROUGH THE DIFFUSIVE LAYER OF THE ARCTIC OCEAN

Angela S. Lefler
Lieutenant Commander, United States Navy
B.S., Texas A&M University, 2003

Submitted in partial fulfillment of the
requirements for the degree of

MASTER OF SCIENCE IN OCEANOGRAPHY

from the

NAVAL POSTGRADUATE SCHOOL
March 2013

Author: Angela S. Lefler

Approved by: Timour Radko
Thesis Advisor

Jason Flanagan
Second Reader

Peter Chu
Chair, Department of Oceanography

THIS PAGE INTENTIONALLY LEFT BLANK

ABSTRACT

The Arctic Ocean has been a subject of increasing interest in recent years due to the reduction of the sea-ice thickness and spatial coverage and its implications for climate change. The future state of the Arctic is likely to be linked to vertical heat transport by microscale processes, specifically, double-diffusive convection. A series of realistic three-dimensional direct numerical simulations (DNS) were conducted to assess the vertical heat transport through thermohaline staircases in the Arctic region. Results revealed that vertical fluxes exceeded those of extant "four-thirds flux laws" by as much as a factor of two, and suggest that the 4/3 exponent requires downward revision. Results also showed that two-dimensional DNS can provide an accurate approximation of heat fluxes when the density ratio is sufficiently large. DNS results also reveal that the models with rigid boundaries result in heat flux estimates that are lower than those from models with periodic boundary conditions. Finally, the DNS-derived flux law was applied to Arctic data and results supported the conclusion that lab-derived flux laws significantly underestimate heat flux. All of these results suggest that vertical heat transport due to double-diffusive convection is a significant contributor to the measured reduction of Arctic sea-ice.

THIS PAGE INTENTIONALLY LEFT BLANK

TABLE OF CONTENTS

THIS PAGE INTENTIONALLY LEFT BLANK

LIST OF FIGURES

LIST OF TABLES

THIS PAGE INTENTIONALLY LEFT BLANK

LIST OF ACRONYMS AND ABBREVIATIONS

AW	Atlantic intermediate-depth Water
CTD	Conductivity Temperature Depth
DDC	Double Diffusive Convection
DoD	Department of Defense
DNS	Direct Numerical Simulation(s)
ERDC	Engineering Research and Development Center
HPCMP	High Performance Computing Modernization Program
ITP	Ice-Tethered Profiler
PADDI	Parallel Algorithm for Double Diffusive Instability
SHEBA	Surface Heat Budget of the Arctic Ocean
TACC	University of Texas at Austin’s Advance Computing Center
T-S	Temperature and Salinity
VAPOR	Visualization and Analysis Platform for Atmospheric, Oceanic and Solar Research
WHOI	Woods Hole Oceanographic Institute

THIS PAGE INTENTIONALLY LEFT BLANK

ACKNOWLEDGMENTS

I would like to thank my advisor, Dr. Timour Radko, for his guidance, infinite patience and commitment to this project. Despite numerous moments of frustration, usually the result of my limited knowledge of program-writing, Timour's energy and optimism never faltered. This patience, coupled with his in-depth knowledge, kept me afloat so that I could see the final, satisfactory results of my project.

I would also like to thank Dr. Jason Flanagan for his programming expertise with Matlab, PADDI, and Linux. Simply put, without his know-how my project would not have been finished. Despite his demanding work schedule, Jason always made time for my programming needs. Thanks must also go to Mike Cook for his assistance with Matlab.

Thanks to my supportive friends and classmates and most importantly, my "Double Diffusion" colleagues. As the last original Angel, I could not have gotten this far without the office pioneers, Erlina and Amy.

This work was supported in part by a grant of computer time from the DoD HPCMP at the ERDC. The Ice-Tethered Profiler (ITP) data were collected and made available by the Ice-Tethered Profiler Program based at the Woods Hole Oceanographic Institution.

Finally, and most importantly, I would like to thank my husband, Brian, for the love and support he provided.

THIS PAGE INTENTIONALLY LEFT BLANK

I. INTRODUCTION AND BACKGROUND

A. ARCTIC OCEAN AND CLIMATE CHANGE

Recent dramatic changes in Arctic sea-ice characteristics, specifically its extent and thickness, have sparked a wide range of scientific interest and concern. There has been greater focus on this fiercely debated subject as research activities increase in response to the reduction in sea-ice coverage. These activities reflect not only the scientific, but also the socioeconomic importance of a reduced Arctic sea-ice region, with increased interest in a wide range of disciplines including merchant shipping, maritime safety and security, and resource management. Figure 1 illustrates the dramatic declination of sea-ice extent, especially in the late summer of 2012 (the dashed line). Combined estimates of ice thickness derived from submarine records, as well as ice, cloud and land elevation satellite laser altimetry, provide a long-term record of sea-ice thickness; these data suggest a decrease in the mean overall thickness of the sea-ice over a region covering about 38% of the Arctic Ocean (Gardner et al. 2012).

Observations suggest that there is a thermodynamic coupling between heat in the ocean interior and sea-ice (Polyakov et al. 2010). This coupling is supported by arguments for the role of oceanic heat in shaping the Arctic sea-ice, linked to the presence of warm intermediate-depth water of Atlantic origin. "Atlantic Water" (AW) carries a vast amount of heat that observations have shown dissipates away from its Arctic entrance, along various spreading pathways.

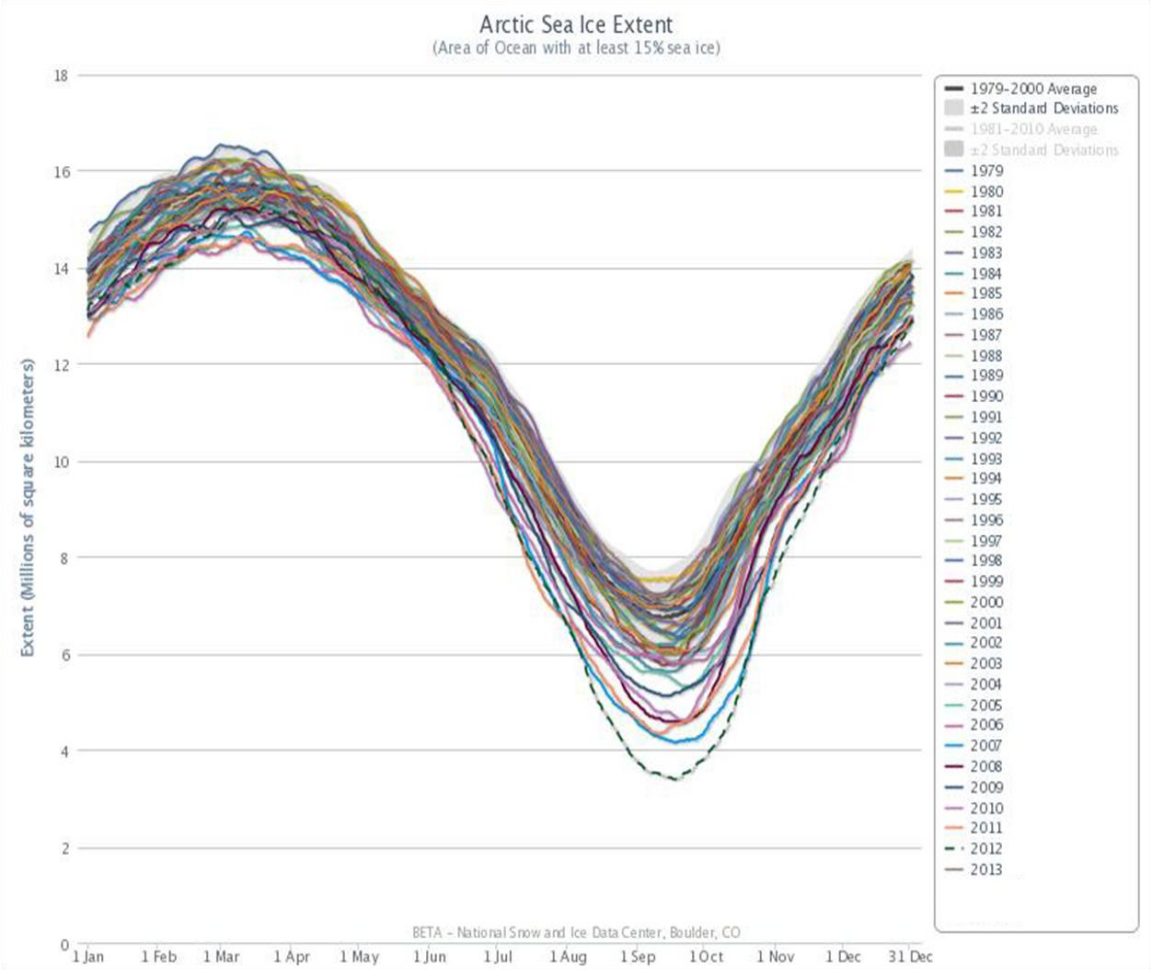

Figure 1. Arctic sea-ice extent declination. Note 2012 data make up the dashed green line (From Fetterer et al. 2012).

While some AW heat is lost along spreading pathways, some of this heat must be lost to the overlying halocline waters (Rudels et al. 1996; Steele and Boyd 1998; Martinson and Steele 2001). Previous analytical estimates of upward heat flux from the AW yield values ranging from 1.3-2.1 W/m^2, while parameterization for the bulk heat transfer coefficient from the mixed layer temperature has yielded vertical heat flux of 3-4 W/m^2 (Krishfield and Perovich 2005). The diversity of these oceanic heat flux estimates can be attributed to strong high-latitude temporal

variability, the various warm and cold periods experienced throughout the twentieth century, and the continually developing understanding of various heat advection mechanisms. AW warms and cools in response to different climate periods, and the remnants of these signals arrive and are felt in the Arctic Ocean years later. Observations from the 2000s document a large-scale warming of the AW layer with temperatures unprecedented in the history of regional instrumental observations (Polyakov et al. 2010).

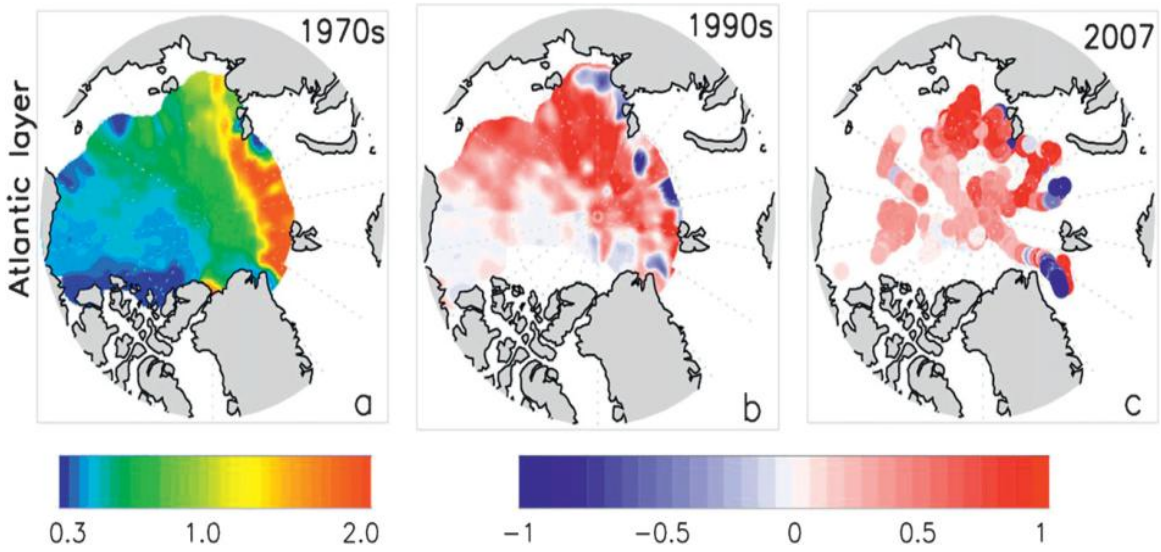

Figure 2. (a) Mean AW temperature (°C) averaged over the 1970s; (b) AW temperature anomalies (°C) averaged over the 1990s, computed relative to the climatological mean; (c) same as (b) but for 2007 data only (From Polyakov et al. 2010).

Using climatology, Figure 2 clearly depicts the anomalously warm AW for the 1990s and more recently, for 2007. At the time, 2007 held the record for minimum summer sea-ice extent in the Arctic region. An anomalous warming event similar to the one documented in 2007 would likely be

observed in 2012; in September 2012, Arctic sea-ice reached a new minimum extent (Figure 1).

It was observed that sea-ice thickness was also shrinking. Regions of the Beaufort and Laptev Seas saw ice-free areas opening faster than before, indicative of the thinner ice melting. Observations from NASA's Operation IceBridge (collection of airborne remote sensing measurements) were used to derive sea-ice thickness and revealed thinning in the Beaufort Sea that could be attributed to warmer AW (Figure 3).

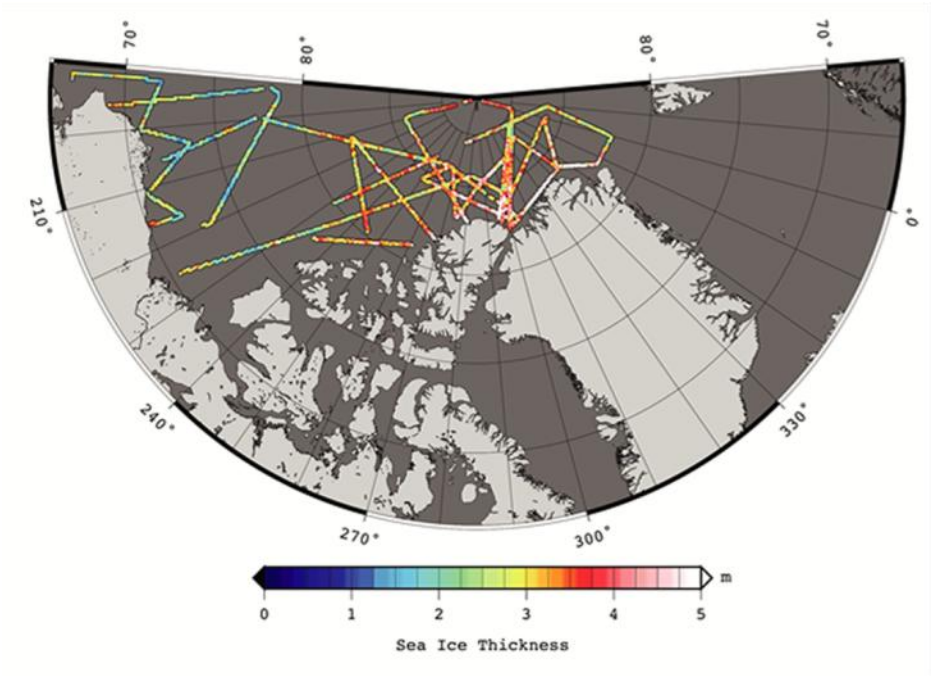

Figure 3. Arctic sea-ice thickness derived from 2012 Operation IceBridge (NSIDC website 2012).

Remote sensing observations also reveal that the thickest (oldest) Arctic sea-ice is thinning and melting at a faster rate than the younger (thinner) ice at the edges of the Arctic Ocean's floating ice cap. Multi-year ice

typically survives the cyclical summer melt season, but this older ice has diminished with each passing winter over the past three decades (Figure 4). The average thickness of the Arctic sea-ice cover is declining because it is rapidly losing its thick component. These dramatic changes point to the possibility of a warmer ocean interior impacting the melting rate of sea-ice.

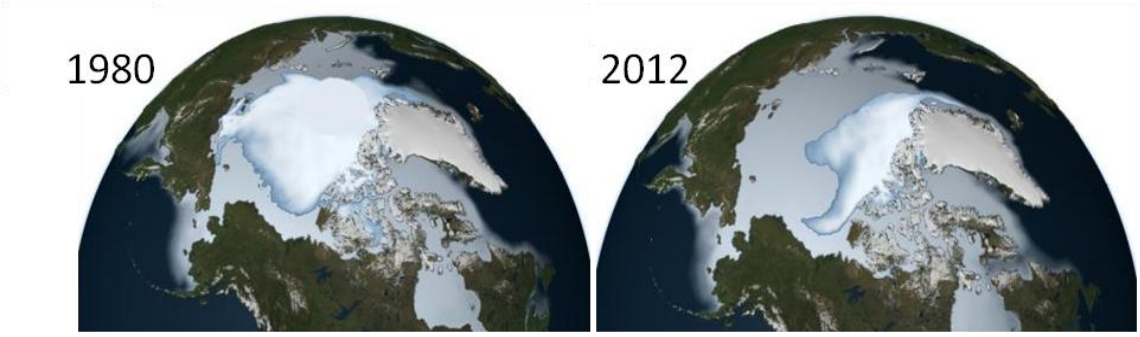

Figure 4. NASA remote sensors show the thickest parts of the Arctic Ice Cap are shrinking (After NASA website 2012).

1. Heat Required to Melt Arctic Sea-Ice

The observed trend of a warming AW layer in the Arctic region, coupled with the irrefutable evidence of shrinking Arctic sea-ice coverage, elicits the question: How significant do these AW temperature changes have to be to impact the upward flux of heat and, in turn, the sea-ice? Additionally, how much heat is needed to melt the sea-ice in the Arctic Ocean, and could it be supplied by the intruding AW? The heat required to melt ice one meter thick is 8 kcal/cm^2 (3.35x10^8 J/m^2) for a latent heat of fusion of 80 cal/gm (Turner 2010). Aagaard and Greisman (1975) have calculated the average net rate of transport of heat into the Arctic by the Atlantic inflow to be about 6.7x10^{10} kW,

with a mean temperature of 2.2 °C. This current accounted for more than half the total heat flux through all passages into the Arctic during a yearlong period (1971-1972). More recent observations find that Aagaard and Greisman's result underestimates subsurface advective heat flux since it does not factor in the more recent increase in temperature of the AW and its extension through the Arctic (Turner 2010).

If the above-referenced heat flux of 6.7×10^{10} kW is distributed uniformly across the entire Arctic Ocean, which has a surface area of approximately 10^7 km^2, and the average heat loss from this layer is about 6.7 W/m^2, then it can be concluded that in 12-18 months there is enough heat in the AW alone to melt one meter of sea ice. Furthermore, there is enough heat from the intruding AW to melt all the sea ice with a mean thickness of 2.5 m in a period of four years (Turner 2010). This assumption is only feasible if there is a mechanism for transferring the heat from the intermediate water level to the surface under the ice pack. These mechanisms that could bring heat from the subsurface layer to the surface over this very short time scale are the subject of several studies (Turner and Veronis 2004).

2. Mechanisms that Impact Melting Rate of Sea Ice

Kwok and Untersteiner (2011) noted that the surplus heat needed to explain the complete loss of Arctic sea-ice during the past few decades is on the order of 1 W/m^2. As the Arctic sea-ice continues to melt at an accelerated rate, the mechanisms responsible for this phenomenon are of increasing interest. Perhaps the most extensively studied mechanism, especially as a target for determining evidence of climate change, is the heat input from the atmosphere

directly to the surface of the ice and the surface mixed layer. Observations gathered during the year-long Surface Heat Budget of the Arctic Ocean (SHEBA) study revealed an annual average net heat flux into undeformed ice of 7.5 W/m^2 (Perovich et al. 2003). The SHEBA values are 2-3 times larger than prior results, which were typically around 3 W/m^2. This increase in atmospheric input can help explain the increased melting rate observed in recent years.

The fact that there is enough heat in the AW to melt all the sea-ice in the Arctic Ocean in just a few years points to the importance of oceanic advective processes that can bring this heat more rapidly to the surface mixed layer. One such mechanism is the mixing caused by the down-flow of dense shelf water. A two dimensional (2D) density current flowing into a two-layer stratified basin will follow along the downward slope, causing a dilution due to the entrainment of lighter fluid above. In the Arctic context, the rejection of brine on the shelves during winter could lead to a dense layer spreading out along the halocline, increasing in density and eventually penetrating below the level of the core of the Atlantic water. This could eventually bring the warmer AW into contact with the surface sea-ice through a combination of upwelling and the erosion of the existing stratification that allows the surface forcing to penetrate more deeply into the water column (Turner 2010).

Another mechanism that impacts the rate of ice-melt was the subject of extensive experimentation by Turner and Veronis (2004). They examined the effect of the vertical transport of heat from warmer layers, intruding laterally

below the surface into a salinity gradient, on the melting sea-ice floating on the surface. The melting rate was found to be dependent on the magnitude of the salinity gradient and on the presence (or absence) of heating from below. The melting rate decreased (increased) as the salinity gradient was increased (decreased). These results demonstrate the potential effect of the vertical double diffusive transport of heat, the mechanism of focus in this thesis.

While solar radiation is undoubtedly the biggest contributor to the reduction of Arctic sea-ice, oceanographic advection processes likely play a much larger role than previously believed, thus explaining the current heat surplus in the Arctic and illustrating the larger role diffusive convection plays in transporting AW vertically to the surface. Figure 5 depicts the interaction of the three primary mechanisms discussed in this section, and the *current* estimates of heat flux, based on previous studies.

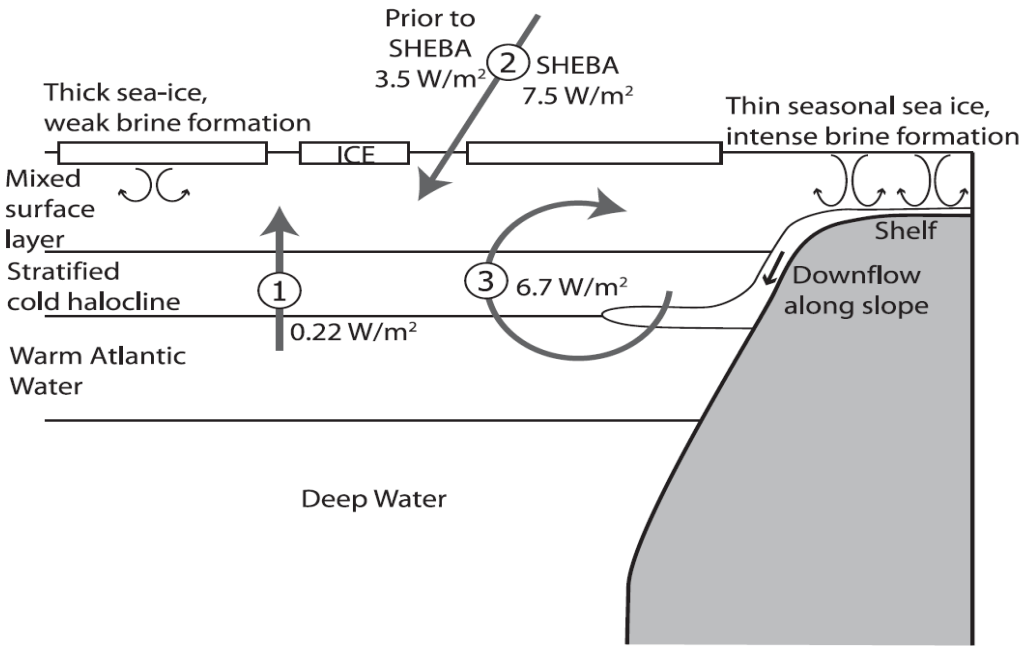

Figure 5. 1: Upward double diffusion transport from the AW. 2: Heat flux from the atmosphere into the surface mixed layer. 3: Mean surface heat flux over the whole region required to balance the net input of heat by the intruding AW (After Turner 2010).

B. DOUBLE-DIFFUSIVE CONVECTION

Turner (1973) describes double-diffusive convection as a phenomenon that occurs in a fluid with two (or more) components with different molecular diffusivities. With regard to the ocean, net differences in the diffusivity of heat and salt are of interest, and give rise to two regimes: salt fingering and diffusive convection.

1. Salt Finger Regime

Salt fingering instability is prevalent in low and mid-latitudes, where the combination of evaporation and radiative heating at the ocean surface results in a layer of warm, salty water overlying a comparatively cooler,

fresher layer of water. These layers are thermally stably stratified, but have an inhomogeneous (destabilizing) composition. Since heat diffuses one hundred times faster than salt, fluid displaced downward rapidly loses its heat excess while maintaining its larger salt concentration. It becomes denser than the surrounding environment and continues to sink, forming salt-finger structures (Figure 6).

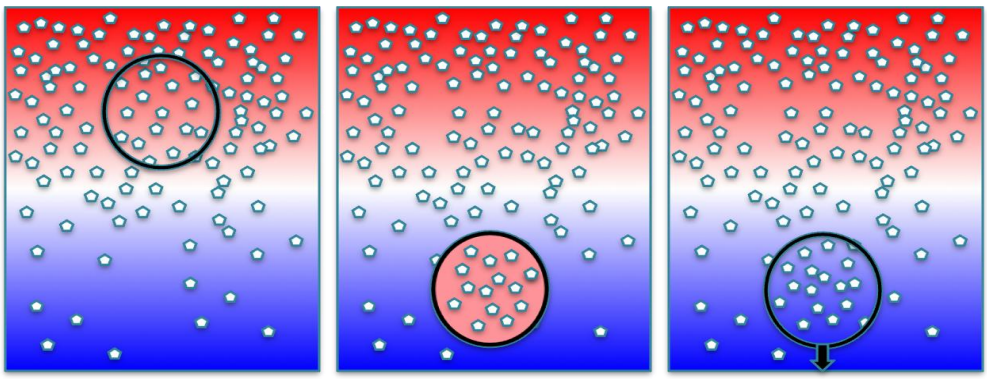

Figure 6. Salt fingers. Warm, salty layer atop a cool, fresh layer results in fingers of salty, cooler water extending downwards from the layer interface (Image from Garaud Research website 2012).

2. Diffusive Convection Regime

In the second case, diffusive instability, the fluid is stably-stratified despite an unstable thermal gradient. It is prevalent in high-latitude locations where cold and fresh water overlies relatively warm and salty water. This phenomenon can occur in the ocean under the ice-shelf, where the slow melting of the ice releases cool fresh water over the warmer, saltier water below. This thesis is focused on the diffusive convection, commonly observed in the Beaufort Gyre region of the Arctic Ocean.

To understand the dynamics of diffusive convection, consider a parcel of warm, salty water that is displaced upward across a thin interface into cooler, fresher water. The parcel quickly diffuses its heat into the new surroundings but slowly releases its salt content. The parcel becomes denser, so it sinks back across the interface and overshoots its original starting point. Now the parcel has returned to warmer waters, and will start this entire process all over again. This over-stable process, known as oscillatory diffusive convection, transports heat upward in an oscillatory fashion (See Figure 7).

This mixing results in the formation of layers of near constant temperature and salinity—diffusive layering. Well-mixed layers separated by sharp diffusive interfaces are responsible for the stair-like appearance of temperature profiles from the central Arctic thermocline. Such profiles are referred to as thermohaline staircases and this process is known to be prevalent in the Beaufort Sea region of the Arctic Ocean. The physical processes associated with the maintenance of this structure are as follows: Heat and salt are transferred upward through the diffusive interface. The water above the interface gains enough heat to begin upward motion due to excess buoyancy. This water begins to rise within the layer, which drives the convection that ultimately maintains the homogeneous properties of the mixed layer. At the same time, the particles just below the interface cool off and sink, which also drives the convection cell in that layer. This process maintains a homogeneous distribution of T-S in each layer (Figure 8). The vertical transport of heat via diffusive layering is the key mechanism of interest being studied in this thesis.

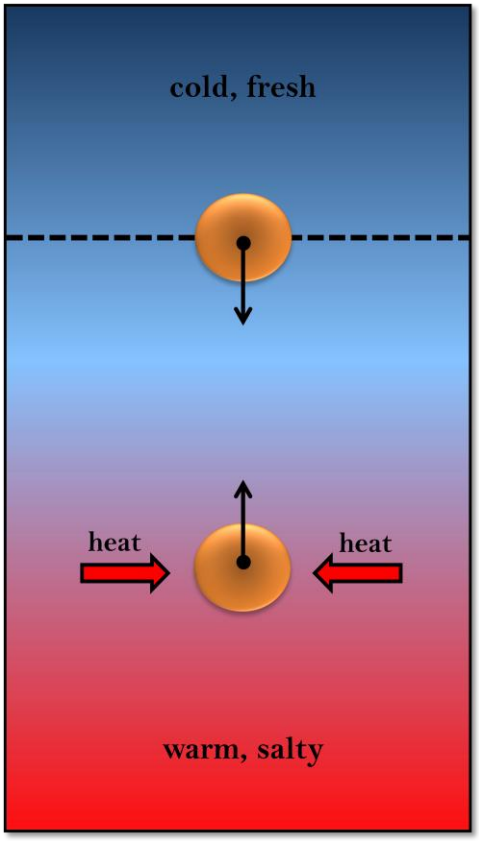

Figure 7. Oscillatory regime. The fluid parcel transports heat vertically.

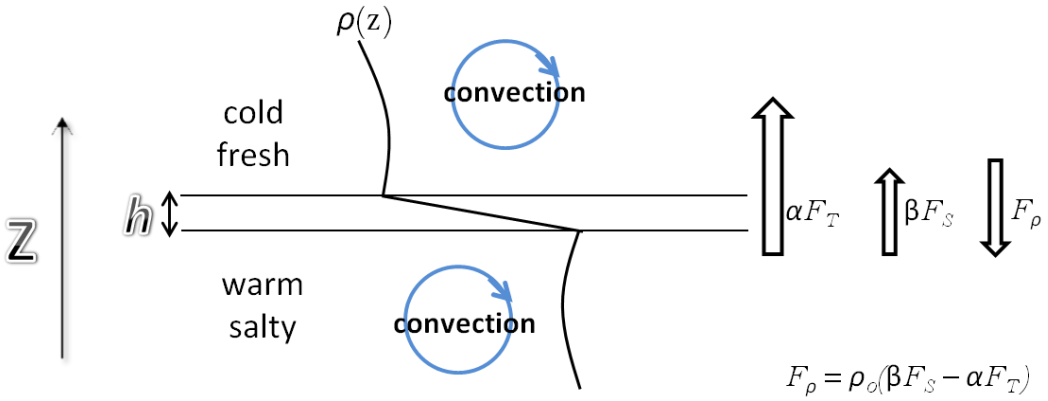

Figure 8. Schematic of the classic thermohaline staircase. Heat convects upward through the interface while the salt transport is limited by its lower molecular diffusivity.

C. FLUX LAWS AND HEAT FLUX ESTIMATES

For systems characterized by active diffusive layering, the interaction between layers is controlled by the salt and heat fluxes across the diffusive interfaces—a dependency that has motivated extensive study. After conducting laboratory experiments, Turner (1965) proposed that the balance of temperature variation between layers and heat flux is given by

$$\alpha F_T = A_1 (\alpha \Delta T)^{\frac{4}{3}} \tag{1}$$

$$R_\rho = \frac{\beta \Delta S}{\alpha \Delta T} \tag{2}$$

Based on the exponent, Equation (1) is commonly referred to as the "four-thirds flux law," where F_T is temperature flux, α is the thermal expansion coefficient, β is the saline contraction coefficient, and A_1 has the dimensions of velocity and is a function of the density ratio (R_ρ). ΔT and ΔS are the differences in temperature and salinity between adjacent layers. This law states that the fluxes associated with double diffusion are controlled entirely by the variation in temperature or salinity across the diffusive interface and is independent of layer thickness. Using dimensional analysis, the 4/3 flux law can be written as

$$\alpha F_T = C(R_\rho) \cdot \left(\frac{g \kappa_T^2}{\nu} \right)^{\frac{1}{3}} \cdot (\alpha \Delta T)^{\frac{4}{3}} \tag{3}$$

where the (unknown) coefficient $C(R_\rho)$ is a function of density ratio only, g=9.8 m/s, $\nu=1.8 \times 10^{-6}$ m^2/s is the kinematic viscosity, and $\kappa=1.4 \times 10^{-7}$ m^2/s is the molecular diffusivity of heat.

In 1976, Marmorino and Caldwell examined Turner's four-thirds flux law in more depth by investigating a larger range of R_ρ values and additional initial conditions. They also factored in Huppert's (1971) heat flux law on interface stability

$$H / H_{sp} = 3.8 R_\rho^{-2} \tag{4}$$

and heat flow

$$H_{sp} = (0.085) k_T \left(g\alpha / \kappa\nu \right)^{\frac{1}{3}} \Delta T^{\frac{4}{3}} \tag{5}$$

through a fictitious non-deformable interface (Turner 1965). Using Huppert's formulae, they determined the relationship between H and H_{sp} to be

$$\frac{H}{H_{sp}} = 0.101 \exp\left\{ 4.6 \exp\left[-0.54 \left(R_\rho - 1 \right) \right] \right\} \tag{6}$$

and proposed the new empirical formulation for the coefficient $C(R_\rho)$

$$C\left(R_\rho \right) = 0.00859 \exp\left(4.6 \exp\left[-0.54 \left\{ R_\rho - 1 \right\} \right] \right) \tag{7}$$

Using empirical formulations, Kelley (1990) found that at low density ratios ($R_\rho<2.5$), temperature fluxes were significantly smaller than those given by Marmorino and Caldwell (1976). This lead to Kelley proposing the formulation

$$C(R_\rho) = 0.0032 \exp\left(4.8 / R_\rho^{0.72} \right) \tag{8}$$

based on what he referred to as a full collection of laboratory experiments; he analyzed experiments for $1 \le R_\rho \le 10$, while Turner (1973) had limited his study to $R_\rho \le 7$.

Kelley also suggested that the exponent to use in Equation (1) be reduced to 5/4. However, (3) with either (7) or (8) continue to be used as a standard method for

calculating fluxes. Additional analysis is required to support or challenge the existing four-thirds flux law.

D. RESEARCH MOTIVATION

This study is focused on the diffusive convection regime of double diffusion. The area of research utilized high resolution three dimensional (3D) numerical modeling aimed at determining the vertical heat transport through double diffusive staircases in the western Arctic Ocean. Direct numerical simulations (DNS) guided and validated attempts to formulate more realistic and accurate heat flux, anticipating that laboratory derived flux laws do not adequately represent the vertical heat transport in the Arctic Ocean. This research determined whether it is possible to reliably assess the performance of flux models using DNS, especially for experiment sizes that most accurately reflect an actual thermohaline step height.

The model runs were high resolution 3D experiments, which were computationally demanding. This higher level of resolution helped determine how accurate earlier 2D numerical models are in terms of predicting vertical heat flux. If, for example, there was not a significant difference in the results between high resolution 3D modeling and 2D modeling, fellow researchers would not worry about acquiring an extensive amount of computational resources. On the other hand, if the results were significantly different, then clearly 2D experimentation is not an adequate approach to modeling this microscale feature.

Another element examined in this study was the role of boundary conditions in controlling the heat transport in staircase models. For example, what form of boundary conditions best represents the dynamics of Arctic staircases? This was simulated by adding boundaries to the DNS that were designed to replicate the restrictions encountered in laboratory experiments. Comparing the results of DNS with periodic and rigid boundaries demonstrated the sensitivity of modeled fluxes to boundary conditions. Finally, the modeled results were validated by incorporating real input values taken from Ice-Tethered Profiler (ITP) data to determine applicability of DNS-derived flux laws in the ocean.

Of note, this is the first series of fully 3D DNS to be performed for the diffusive convection for the step-size and diffusivity ratio that is representative of Arctic staircases. It was anticipated that DNS-derived flux values would be significantly higher than those previously encountered in laboratory experiments, and that it is feasible for vertical heat transport via double diffusion to be significant enough to impact the melting of Arctic sea-ice.

II. MODEL DESCRIPTION AND SETUP

DNS were conducted in both two and three dimensions. Lower resolution, 2D experiments were conducted on the Naval Postgraduate School (NPS) high-performance Hamming Linux cluster using between 64 and 256 processors per run. 3D model runs were performed on the Department of Defense's High Performance Computing Modernization Program (HPCMP) Open Research Systems, Cray XE6 (Chugach) and Cray XE6m (Copper) located at the Engineer Research and Development Center (ERDC) in Vicksburg, MS; and on the University of Texas at Austin's Advance Computing Center (TACC) using their Sun Constellation Linux Cluster (Ranger), and their Dell Linux Cluster (Lonestar). The resources used varied from 256-2048 processors per run for computing and model efficiency testing; results determined that 512 processors are optimal for final high resolution runs.

The simulations were performed using the Parallel Algorithm for Double Diffusive Instability (PADDI) model, a fully de-aliased, pseudo-spectral, Fortran numerical code developed specifically for double diffusive convection and which utilizes a domain that is periodic in each spatial dimension (L_x, L_y, L_z). The model was parallelized using the Message Passing Interface (MPI), and code was compiled using the Intel Fortran compiler. Experiments were run in single precision once it was verified that the differences between single and double precision results were not significant. The 2D study examined diffusive convection in the horizontal (x) and vertical (z) directions.

For modeling purposes, temperature and salinity output fields were decomposed into the linear basic state $(\bar{T},\bar{S})$ and perturbations (T,S). The relevant equations are then the Boussinesq equations of motion, expressed in terms of T and S and non-dimensionalized using the "standard" double-diffusive system (Radko 2013):

$$l = (\frac{\kappa_T \nu}{g\alpha \bar{T}_z})^{\frac{1}{4}} \tag{9}$$

$$v = \frac{\kappa_T}{l} \tag{10}$$

$$t = \frac{l^2}{\kappa_T} \tag{11}$$

Here, l denotes the length scale, v is the velocity scale, t is the time scale, T_z is the temperature gradient and $\alpha T_z l$ is the scale for both temperature and salinity perturbations (Radko and Stern 1999). These relationships lead to the following governing non-dimensional equations that are solved by PADDI

$$\frac{1}{Pr}(\frac{\partial \mathbf{u}}{\partial t} + \mathbf{u}\cdot\nabla\mathbf{u}) = -\nabla p + (T - S)\mathbf{k} + \nabla^2\mathbf{u} \tag{12}$$

$$\nabla\cdot\mathbf{u} = 0 \tag{13}$$

$$\frac{\partial T}{\partial t} + \mathbf{u}\cdot\nabla T - \mathbf{k}\cdot\mathbf{u} = \nabla^2 T \tag{14}$$

$$\frac{\partial S}{\partial t} + \mathbf{u}\cdot\nabla S - R_\rho \mathbf{k}\cdot\mathbf{u} = \tau\nabla^2 S \tag{15}$$

for initial conditions representing the system at rest

$$\mathbf{u}(\mathbf{r}, t = 0) \tag{16}$$

where the step-like distribution of temperature and salinity are the result of slight perturbations caused by random computer-generated noise.

Equation (12) is the equation of state, Equation (13) is the continuity equation, and Equations (14) and (15) are the thermal and compositional advection-diffusion equations. Here, **u** denotes the velocity field and p is pressure (Peyret 2002; Canuto et al. 2007; Stellmach and Hansen 2008). Equations (12)-(15) can be solved in either a 2D or 3D periodic domain, thereby representing conditions in the real ocean where the influence of boundary conditions are minimal. The governing parameters are the Prandtl number (Pr), molecular diffusivity ratio (τ), and R_ρ. Pr and τ are defined as

$$\mathrm{Pr} = \frac{\nu}{\kappa_T} \tag{17}$$

$$\tau = \frac{\kappa_S}{\kappa_T} \tag{18}$$

where κ_T is the molecular diffusivity of heat and κ_S is the molecular diffusivity of salt.

One-layer DNS were conducted using parameter settings that reflect those found in the vicinity of the Beaufort Gyre in the Arctic Ocean, where recently, ITPs have recorded temperature and salinity profiles that clearly show stepped patterns at depths 200-300 m (Timmermans et al. 2008). Therefore, for all experiments, $\nu=1.8\times10^{-6}$ m^2/s, $\kappa_T=1.8\times10^{-6}$ m^2/s, $\kappa_S=7\times10^{-10}$ m^2/s, yielding $\tau=0.005$ and Pr=13. Previous DNS were unable to use such a small τ value because of the computational difficulty of resolving the extremely fine salt dissipation scale (e.g. Prikasky 2007;

Caro 2009; Carpenter et al. 2012). From ITP data, the average values $\alpha=5.625\times10^{-5}$ 1/°C and $\overline{T_z}=1.361\times10^{-2}$ °C/m were determined over the appropriate depth range. Thus, $l=1.35\times10^{-2}$ m and the relevant non-dimensional layer-thickness range is 74–740. The density ratio in the diffusive layer of the Arctic Ocean is typically in the range $2\leq R_\rho\leq10$ and this analysis is based on a series of experiments with $R_\rho=[2,3,4,6,8,10]$.

For 2D experiments, the chosen non-dimensional domain size was 300x300 so as to reflect step-sizes in an actual Arctic staircase. The corresponding mesh size was 756x3072 to sufficiently resolve the scale of salt dissipation for the realistic diffusivity ratio used. For 3D experiments, the typical non-dimensional domain size was 300x150X300 and the corresponding mesh size was 756x384x3072. The box size, H, is varied in one set of 2D and 3D experiments.

One further experiment, designed to replicate imposed laboratory-type boundary conditions and observe their influence on vertical heat transport in thermohaline staircases, was conducted. For this experiment, rigid stress-free boundaries were assumed in all spatial dimensions, with minimal changes to the underlying code. Table 1 outlines all the DNS conducted in this study.

2/3D	Type	Size (m)	Mesh Size	τ	Rρ	Total # of experiments
3D	Periodic	4x2x4	768x384 x3072	.005	2,3,4,6,8,10	6
3D	Periodic	4x2x2	768x384x1536	.005	4	1
3D	Periodic	4x2x1	768x384x768	.005	4	1
3D	Periodic	4x2x0.5	768x384x384	.005	4	1
2D	Periodic	4x4	768x3072	.005	2,3,4,6,8,10	6
2D	Periodic	4x2	768x1536	.005	4	1
2D	Periodic	4x1	768x768	.005	4	1
2D	Periodic	4x0.5	768x384	.005	4	1
2D	Non-periodic	4x4	768x3072	.005	1.5+	1

Table 1. A list of DNS conducted in this study.

Prior to this study, the computational demands of performing DNS in 3D led modelers to either resort to 2D simulations or to compromise in their choice of parameters (use unrealistic values of diffusivity ratio or step heights, for instance). Caro (2009) performed DNS of a fluid with periodic boundary conditions but with unrealistic τ and H values (relative to what is typically observed in the Arctic Ocean) because he found using smaller diffusivity ratios and larger grid sizes to be computationally prohibitive. Because of these limitations, he extrapolated high-tau simulations to evaluate the vertical heat transport for Arctic conditions and still found it to be significantly larger than inferred from laboratory experiments. He concluded that laboratory experiments being conducted in small tanks that have rigid boundaries would have quite different parameter ranges and were very susceptible to experimental errors.

Carpenter et al. (2012) also performed a series of three-dimensional DNS, but at a significantly higher resolution, utilizing a larger domain (L_x, L_y, L_z) and mesh size, and a more realistic range of τ. Their results also showed that the flux laws of Kelley (1990) gave lower predicted fluxes than those observed in their simulations, with a stronger dependence on density ratio. Their experiments also had imposed unrealistic rigid boundary conditions that might have stunted the flux values. Both Caro's (2009) and Carpenter et al.'s (2012) results bring into question the relevance of lab-based flux laws when applied to Arctic staircases.

To that end, the key to this study was to incorporate all the relevant parameters and measures that would most accurately represent a typical Arctic thermohaline step. To date, no 3D DNS has simultaneously utilized a mesh size that sufficiently resolves the scale of salt dissipation for a realistic τ=.005; increased domain size to accurately reflect step-sizes in an actual staircase (H~4 m); allowed the DNS to run for a time period that ensures accurate diagnostics; and guaranteed that all parameters and conditions, such as a lack of rigid boundaries, are reflective of those found in the Arctic. Such a set-up required an unprecedented amount of resources but produced flux law derivations that are more representative of real-world conditions.

III. MODEL RESULTS

A. TWO-DIMENSIONAL MODEL

1. General Characteristics

Modeling in 2D served three purposes. First, it provided a testing platform for checking all the parameters, and ensured the model output met expectations prior to running the equivalent 3D jobs (e.g. flux trends and dependencies). As anticipated, computational resources needed for running high resolution 3D jobs were limited and could not be wasted. Second, 2D model runs were conducted so that the results could be compared to their 3D counterparts to determine the dependencies of heat flux on step heights (H) and R_ρ. Finally, the last, rigid boundary model run was completed in 2D in favor of its numerical efficiency. Refer to Table 1 for the complete details of the 10 experiments ran in 2D.

Figures 9-11 show a full temperature field plot revealing the spatial structure of the diffusive convection. The two layered fluid is initially at rest (Figure 9), with no activity across the single interface. Higher temperature values are shown in red and lower values in blue. Figure 10 depicts signs of initial convective activity across the interface as the heat exchange begins to diffuse between the two layers. Figure 11 more clearly shows the heat signatures of active transport and the temperature field becoming better mixed just above and below the interface. In Figure 11, the field is "zoomed in" on a particular area of the interface to better show the

detail of enhanced convective dynamics, further confirmed by plumes emanating from the interface.

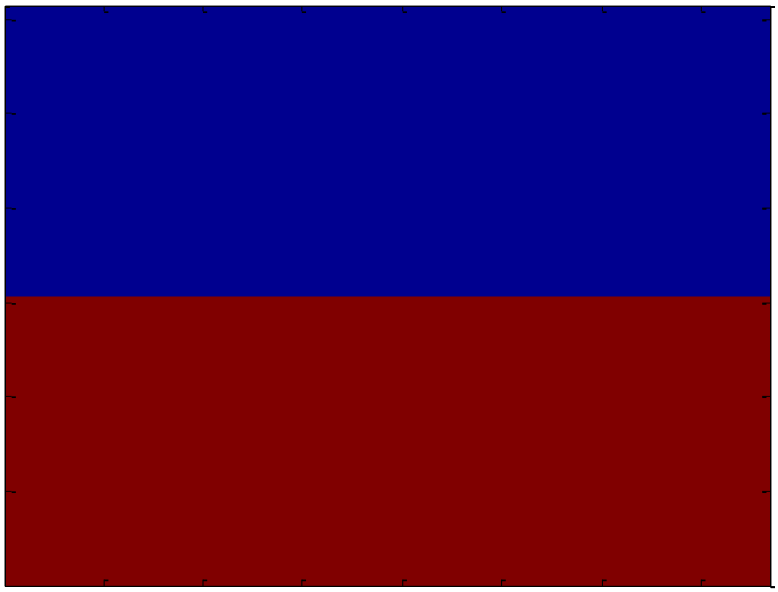

Figure 9. 2D temperature field at t=0. Simulation is at rest and no convection has begun. Plot aligns with the x-z axis (not to scale).

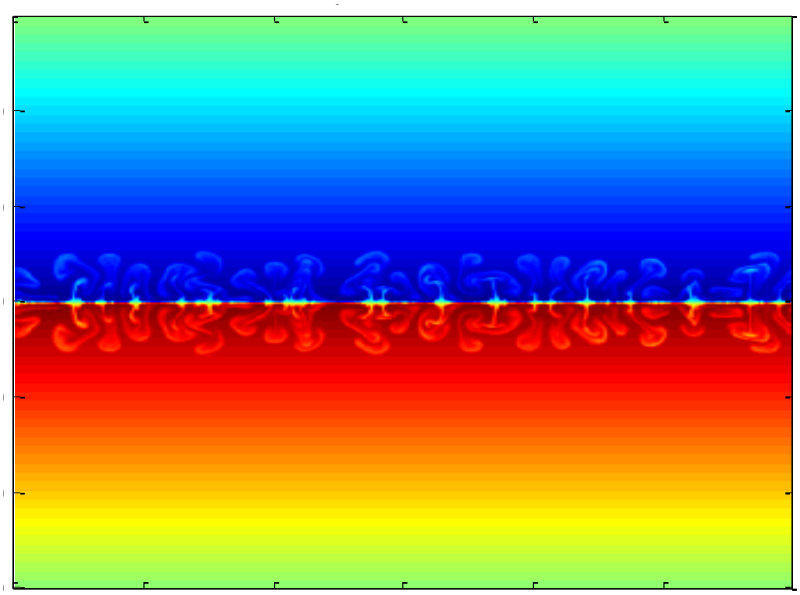

Figure 10. 2D temperature perturbation field at t=27 minutes. Convective plumes become visible in both layers.

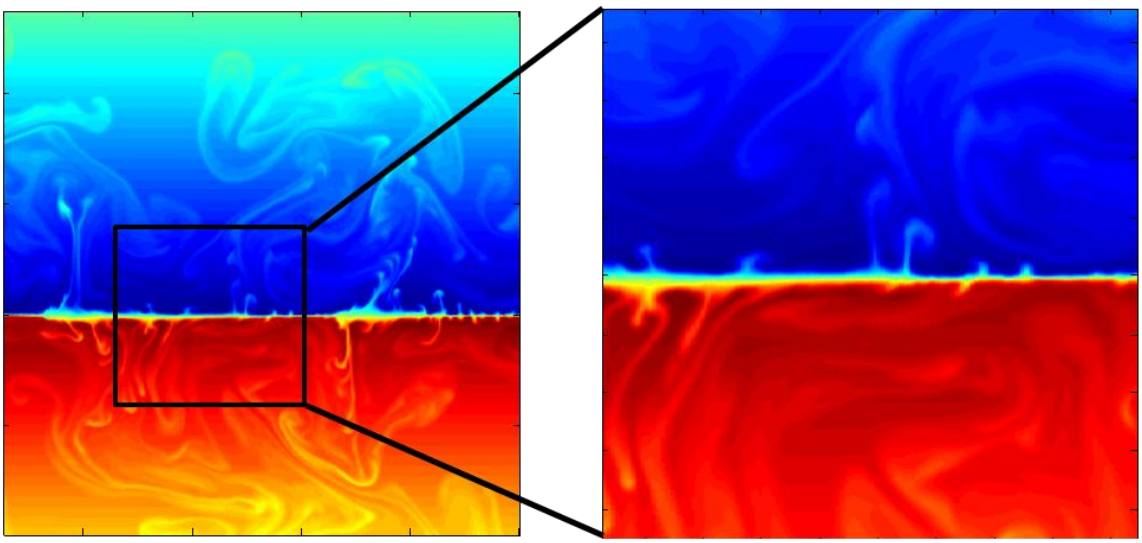

Figure 11. 2D temperature perturbation field plot at t=1.3 hours. View is zoomed in from left to right, showing further detail of the convective dynamic.

2. Flux Trends and Dependencies

Temperature flux averaged over the whole computational domain was recorded and smoothed in time using the running average period of 20 non-dimensional units to remove high-frequency oscillations. Figure 12 shows the typical evolution of heat flux as a function of time. The simulation is initiated at rest, followed by random noise "kicking" off the double-diffusion process. This is why there is strong flux growth almost immediately after the simulation begins, indicative of a large amount of potential energy being released by the temperature field. As time increases the system reaches a state of near-equilibrium, with fluxes fluctuating about a mean value. In this thesis, the mean heat fluxes were determined from the equilibrated portion of the graph.

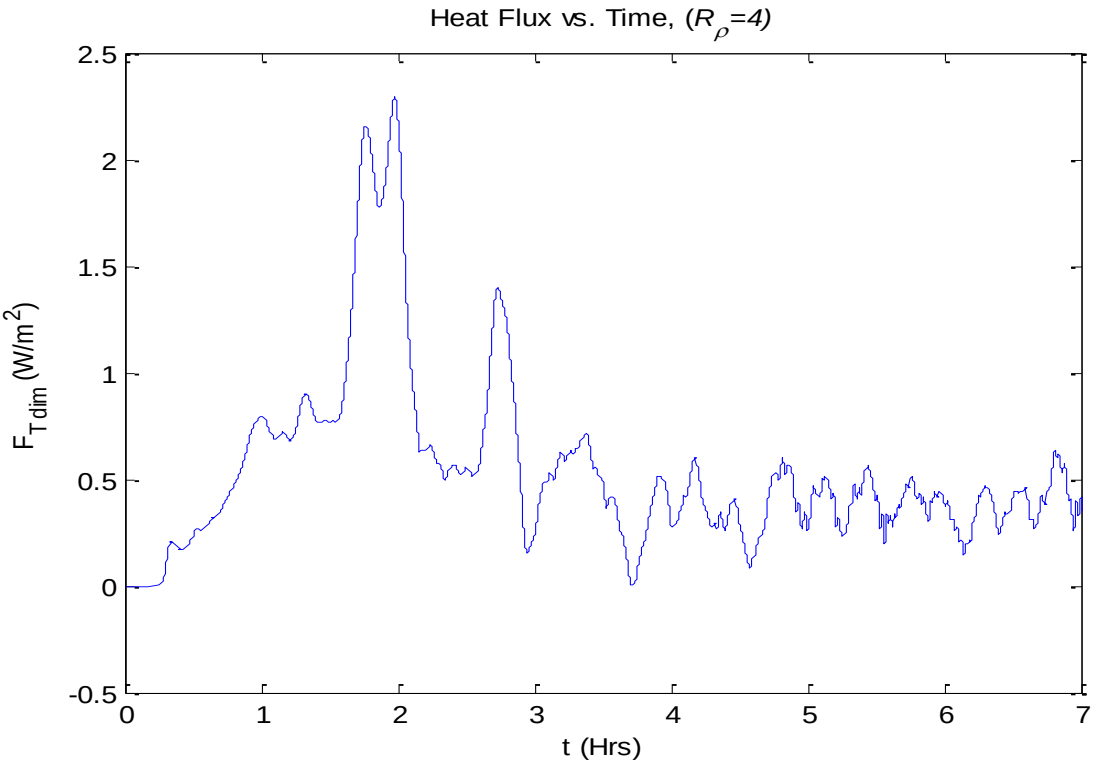

Figure 12. A typical evolutionary pattern of temperature fluxes as observed in simulations. Taken from the experiment with R_ρ=4.

Through one-step numerical experiments, it is possible to determine the magnitude of diffusive fluxes and compare them with those derived from laboratory experiments. Since DNS flux results are non-dimensional, a conversion was made to get dimensional units. Non-dimensional and dimensional DNS temperature fluxes are related by

$$F_{T\,\mathrm{dim}} = F_{T\mathrm{non-dim}} \kappa_T \frac{dT}{dz} \tag{19}$$

with the corresponding (dimensional) heat flux given by

$$F_{H\,\mathrm{dim}} = F_{T\,\mathrm{dim}} C_p \rho \tag{20}$$

where C_p is the specific heat for sea water and ρ is the density of sea water. Substituting (19) into (20) and

utilizing values calculated from ITP data for the Beaufort Gyre yields a conversion factor of 0.0075 W/m^2 (Prikasky 2007; Caro 2009).

As indicated by Equations (1)-(3), fluxes are expected to be dependent on the density ratio for a fluid with a temperature variation across the interface (Turner 1973). To determine this dependency, six one-layer DNS were performed, each with a different R_ρ chosen from [2,3,4,6,8,10] and H_{nondim}=300 (~4 m in dimensional units). Each DNS illustrated the same behavior as seen in Figure 12. As expected, fluxes consistently decreased with increasing Rρ, with measured values F_{Hdim}=[0.634,0.527,0.398,0.360,0.316,0.300] W/m^2.

To determine flux dependency on H, four one-layer DNS were performed for H_{nondim}=[37.5,75,150,300], equivalent to approximate dimensional values of H_{dim}=[0.5,1,2,4] m, and fixed R_ρ=4. An increase in H for fixed temperature gradient corresponds to variation in ΔT, thus allowing systematic analysis of the corresponding pattern of variation of heat transport. As anticipated, fluxes increased with the increasing layer thickness, with F_{Hdim}=[0.053,0.102,0.204,0.398] W/m^2.

These dependencies, and how they compare to laboratory experiment results, are discussed next in greater detail, in the context of 3D DNS.

B. THREE-DIMENSIONAL MODEL

Figure 13 presents the typical distribution of the total temperature ($\bar{T}+T$) field realized in 3D DNS. This visualization reflects the interaction between regular,

nearly flat interfaces and disorganized convective plumes advecting temperature and salinity through well-mixed layers. Shown are two identical layers to illustrate the periodic nature of the system (based on a single layer DNS).

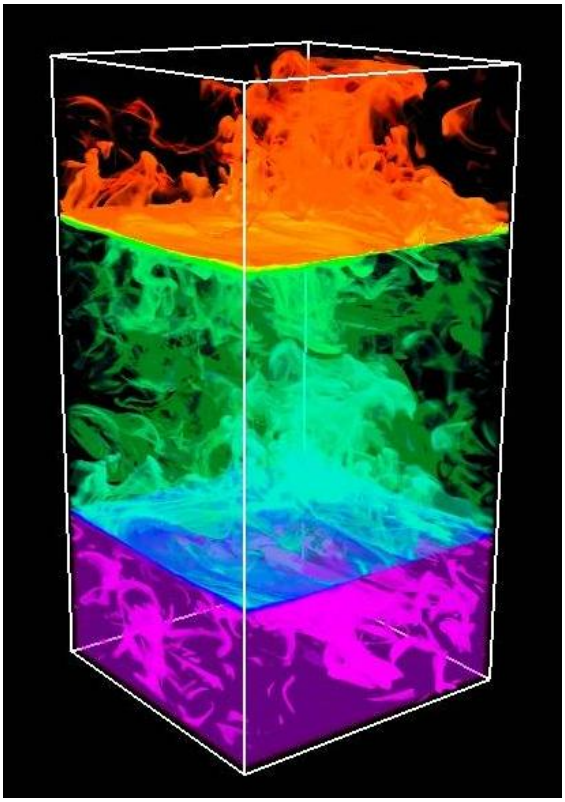

Figure 13. 3D volume rendering of a diffusive convection temperature field for R_ρ=4. Graphic generated using VAPOR software.

As was the case with 2D DNS, a series of 3D experiments were performed in the configuration that is consistent with typical staircases in the Beaufort Gyre of the Arctic Ocean for various density ratios, R_ρ=[2,3,4,6,8,10] and step heights, H_{dim}=[0.5,1,2,4] m. Refer to Table 1 for further details on these nine experiments. As expected, heat flux values for each DNS evolved in the

manner illustrated in Figure 12. Thus, the same procedure for calculating mean fluxes applied to 2D experimentation could be used for all DNS, over similar time intervals (thereby ensuring consistency in our approach).

1. Flux Law Comparisons

Marmorino and Caldwell's (1976) and Kelley's (1990) lab-derived formulations of the 4/3 flux law (Equations (7) and (8), respectively), were used for comparison with the 3D DNS results. Figure 14 compares heat fluxes diagnosed from the DNS with those derived using the 4/3 flux law for a range of density ratios. This comparison indicates that for low R_ρ, laboratory estimates enjoy some success in estimating heat flux (F_H). For instance, at R_ρ=2, Kelley's (1990) law is within 10% of the DNS value, with Marmorino and Caldwell's (1976) law performing at a similar level for R_ρ=3. However, for larger R_ρ (>~3), both laws underestimate F_H, with the discrepancy increasing with R_ρ. An approximate factor of 2 difference can be seen at large values of density ratio (R_ρ>5). This discrepancy is not surprising, given the substantial differences in the numerical and laboratory setup.

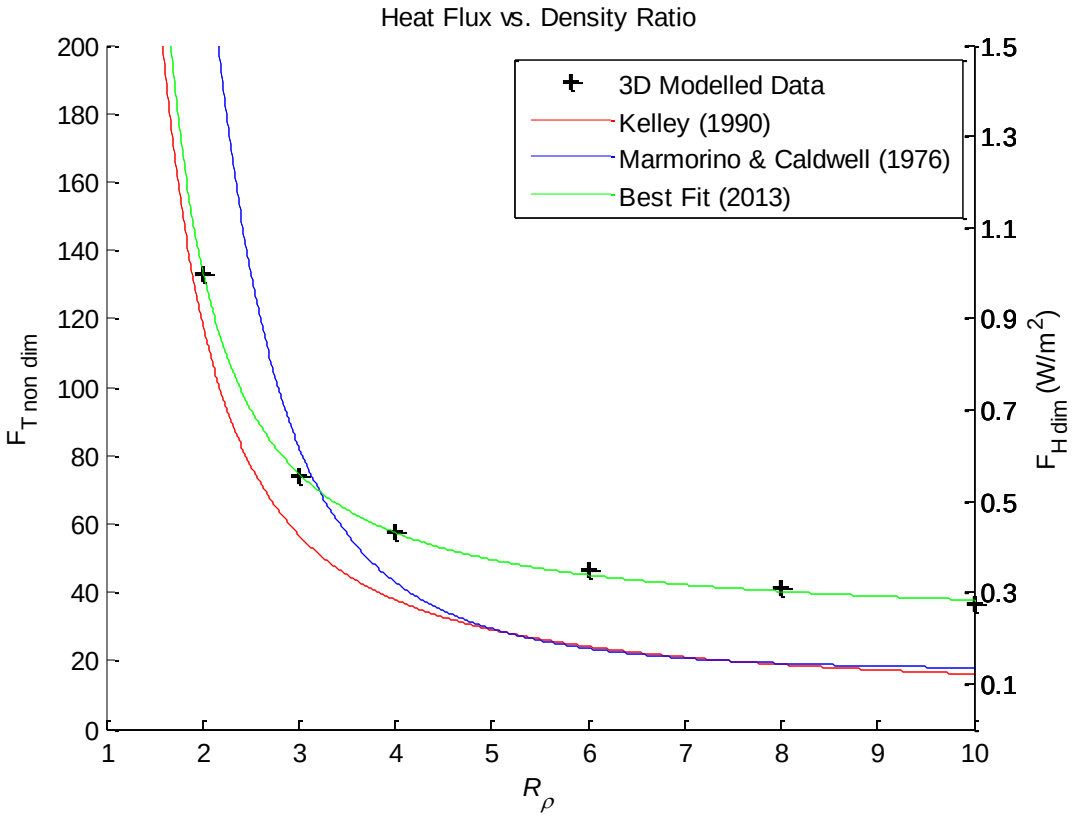

Figure 14. A comparison of heat fluxes (as a function of R_ρ) diagnosed from 3D DNS with those derived from extant laboratory-derived flux laws.

In order to present the DNS findings in explicit form, also presented in Figure 14 is the best-fit curve of the form

$$F_{T\text{non dim}} = a + b(R_\rho - 1)^C \qquad (21)$$

where a=31, b=103.4 and c=-1.24. If we additionally assume that, at the leading order, the dependence on ΔT follows the four-thirds power law, then (21) leads to the following parameterization of vertical transport

$$\alpha F_{T\text{dim}} = [a_1 + b_1(R_\rho - 1)^c](\alpha \Delta T)^{4/3} \qquad (22)$$

The discrepancy in the lab-derived flux values in calculating fluxes points to an inaccurate prefactor value,

with an error of 2-3. Note that Equation (22) offers an adequate description of the numerical data provided that the dependence on temperature variation is well-described by the 4/3 power law. Whether or not this assumption is accurate can also be questioned (Kelley et al. 2003).

2. Testing the 4/3 Exponent

In order to determine whether the numerical simulations are adequately represented by the 4/3 power law in Equation (3), a set of four one-step 3D DNS with different step-heights was performed with varying H and fixed R_ρ=4. All other parameter settings were kept identical for each. The increase in H for the fixed temperature gradient (T_z=1.361x10^{-2} °C/m) corresponded to the variation in ΔT. Figure 15 is the plot of αF_T as a function of αΔT (dimensional units) in logarithmic coordinates as derived from DNS and as estimated by Kelley's (1990) law. From inspection of Figure 15, it is immediately apparent that the 4/3 exponent does not accurately describe the numerical results. A best-fit curve of the form

$$\log(\alpha F_T) = c + m\log(\alpha \Delta T) \tag{23}$$

yields m=1.02 (with c=−13), which is significantly less than the commonly assumed 4/3. If the fit is made so as to exclude the lowest αΔT, then m=1.11. It also should be noted that laboratory flux estimates came close to the numerical values for relatively large ΔT (equivalent to large step heights, H), but differed for relatively thin steps.

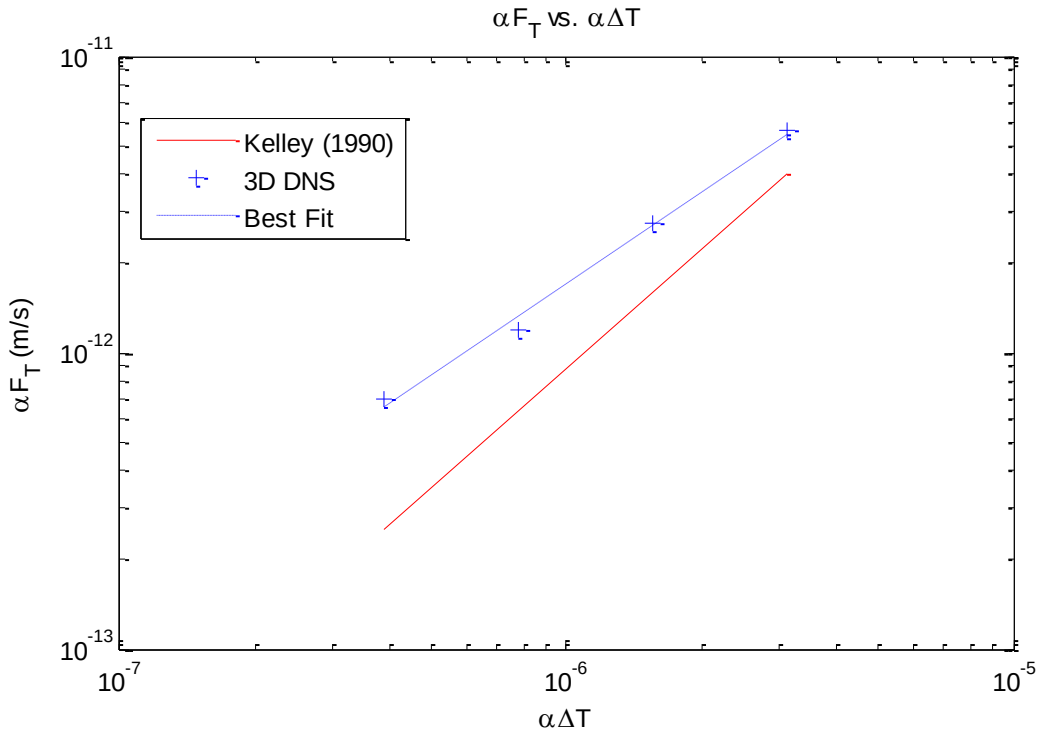

Figure 15. Testing "four-thirds flux law" exponent. αF_T (m/s) as a function of $\alpha\Delta T$ in logarithmic coordinates, as diagnosed from 3D DNS.

C. COMPARISON OF TWO- AND THREE-DIMENSIONAL EXPERIMENTS

Utilizing 2D DNS has its obvious advantages, especially in a computationally-restrictive modeling environment. 2D DNS are less expensive for realistic parameters, but it is reasonable to question whether they provide adequate approximation to their 3D counterparts. For instance, it is widely-known (e.g. Kolmogorov 1941; Batchelor 1953) that energy cascades from larger to smaller scales in the full 3D regime whereas the opposite is true for 2D simulations. To test their accuracy, 2D DNS with identical parameter sets and resolutions to those 3D DNS previously described were conducted. Mean temperature fluxes were noted and compared by looking at the resultant

3D/2D ratios ($\bar{F}_{T3D}/\bar{F}_{T2D}$). Figure 16 shows this ratio for the DNS with varying R_ρ and fixed H (top panel), and varying H and fixed R_ρ=4 (bottom panel).

Surprisingly, in both cases, 2D DNS stand up quite well. For varying R_ρ, the maximum value $\bar{F}_{T3D}/\bar{F}_{T2D}$=1.574 occurs at R_ρ=2. However, for all larger R_ρ values, 2D estimates are within 10% of their 3D counterparts. The same consistency between 2D and 3D results is seen when density ratio is kept constant and layer thickness is systemically varied.

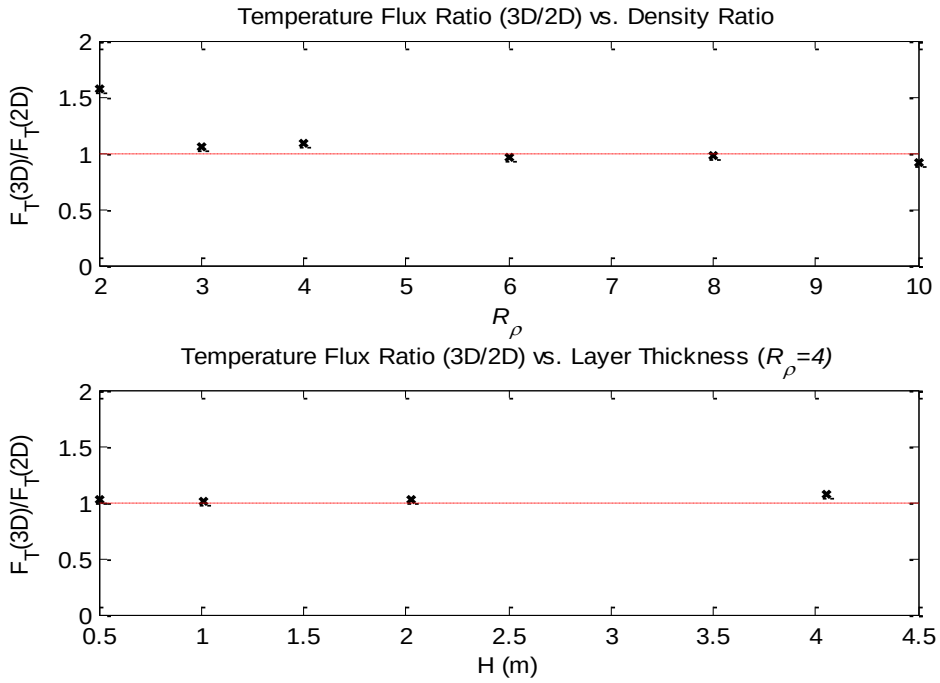

Figure 16. Comparison of 3D and 2D DNS as a function of R_ρ (top panel) and H (bottom panel). With the exception of R_ρ=2, the 3D/2D ratios were within 10% of $\bar{F}_{T3D}/\bar{F}_{T2D}$=1.

D. EFFECTS OF BOUNDARY CONDITIONS

Carpenter et al. (2012) performed a series of 3D DNS which differed from those of Caro (2009) in that their model configuration included *rigid* boundaries. As a result, their DNS experienced a run-down evolution of the diffusive interface, a feature that is compatible with the laboratory configuration but which may not be realized in actual oceanic staircases. Although Carpenter et al. (2012) showed that the laboratory-based flux laws predict lower heat transport than those observed in their simulations, it is likely that their derived flux values are still too low because of the implementation of rigid boundary conditions.

To test the effects of boundaries, a numerical experiment with rigid stress-free boundaries in all spatial directions was conducted; the setup that reflects the dynamics of a laboratory run-down experiment. The DNS were run in two dimensions only, since they have been shown to be generally adequate in capturing the dynamics of diffusive convection and the associated heat transport. To make the comparison between the periodic and run-down simulations objective, in both cases the same parameters were used (see Table 1). At initialization, R_ρ=1.5, and as the system ran down, R_ρ increased with time. This made it possible to calculate the mean temperature flux as a function of density ratio over the continuous range $1.5<R_\rho<10$.

In Figure 17 heat flux values as a function of R_ρ from this DNS are compared to those derived from the periodic 2D simulations. In the run-down experiments, heat flux was computed at the level of diffusive interface (z=H/2) and

smoothed in time using the running average interval of 100. For smaller values of R_ρ (<3), fluxes with rigid boundaries are larger with the difference rapidly diminishing as R_ρ increases. Quickly, the run-down fluxes fall significantly below the corresponding estimates from the periodic simulations. For comparison purposes, flux values as determined by Kelley's (1990) law were included. As is to be expected from a flux-law obtained in the laboratory setting (where rigid boundaries are present), Kelley's law provides better overall approximation to the run-down DNS-based flux values, than the periodic system.

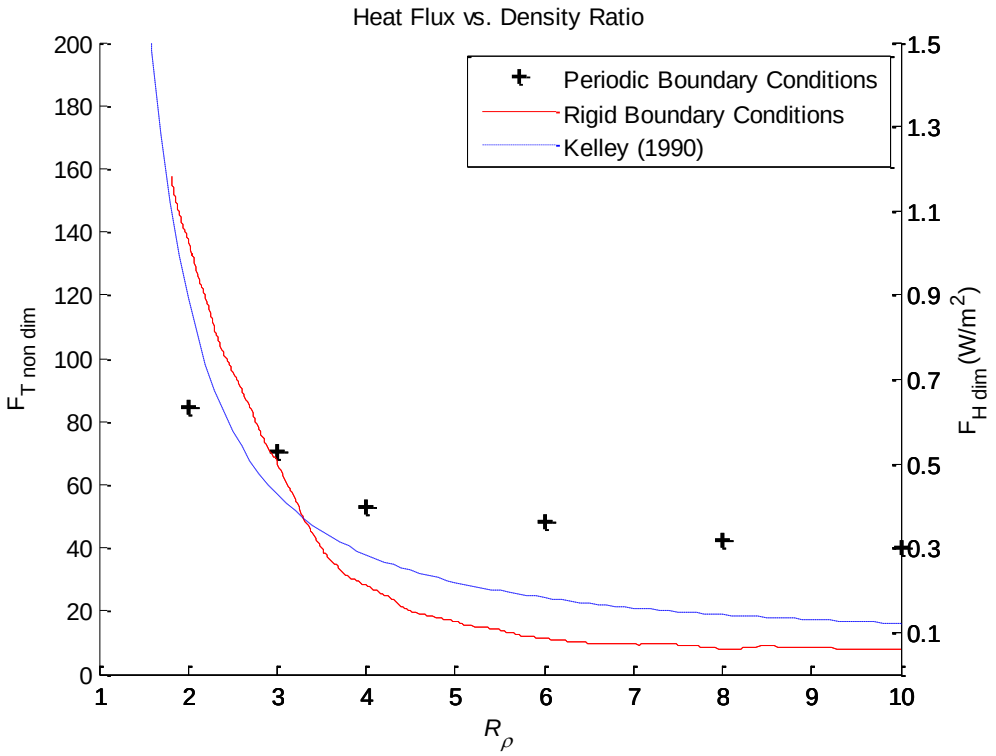

Figure 17. The effect of boundary conditions as seen when comparing fluxes as a function of R_ρ. As R_ρ increases, fluxes without boundaries are significantly higher than their non-periodic counterparts.

This DNS demonstrates the inherent difficulties that arise when studying diffusive convection in a laboratory setting. The rigid boundaries and/or run-down character of experiments act to significantly suppress the vertical heat transport. Since a rigid bottom and side-walls are present in laboratory experiments, the application of the laboratory-derived flux laws to oceanic interfaces, which are not constrained by rigid boundaries and which can persist for years, may not be appropriate. Based on the high-resolution experiments with periodic boundary conditions it is estimated that the error of extant flux laws is modest (a factor of two or less) and could be tolerated in many applications. However, if a more accurate estimate of the vertical heat transport is needed, using Equation (22) is recommended, since it is based on the periodic simulation results.

IV. DATA AND DATA PROCESSING

A. ICE-TETHERED PROFILERS AND PREVIOUS RESEARCH

The Woods Hole Oceanographic Institute (WHOI) ITP program provides timely and accurate oceanographic measurements from the Arctic Ocean. ITPs assist in assuring consistent measuring capability in regions that have, until now, remained data-sparse due to access limitations. The ITP is a moored conductivity, temperature, and depth (CTD) sensor that returns high vertical resolution measurements of upper ocean temperature and salinity beneath sea-ice. Each one is designed to move with the ice it is moored to and consists of a small platform on top of which rests a buoy. A 10-inch hole is drilled through the sea ice and the instrument is inserted in the water from above. The instrumentation is tethered to the surface float via a wire rope that is weighted on the bottom. This rope is approximately 800 meters in length, and the instrument traverses the wire rope several times daily (Figure 18).

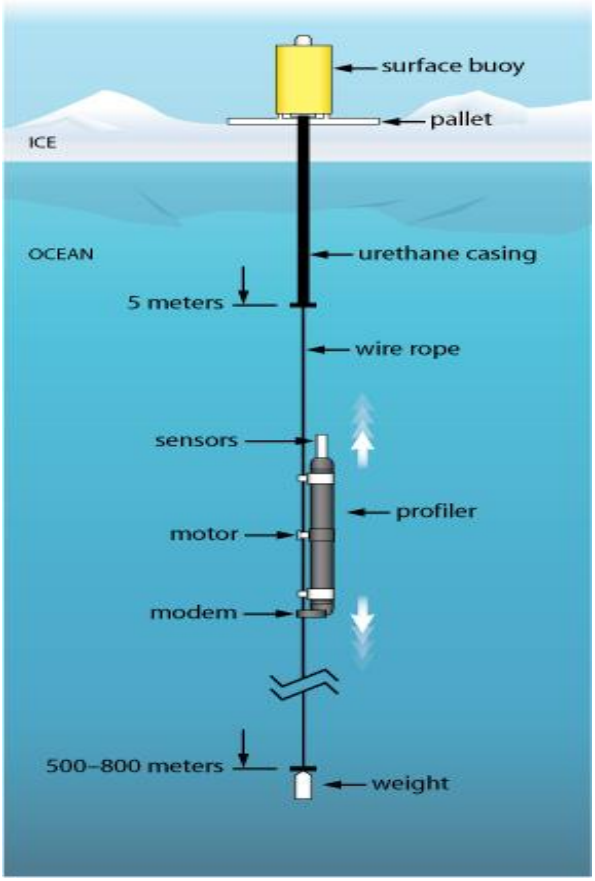

Figure 18. Ice-Tethered Profiler (ITP) schematic (WHOI ITP website 2012).

Data from ITPs 1-6 were used for comparison with previous studies that focused on the double-diffusive staircases in the Beaufort Gyre (e.g. Timmermans et al. 2008; Caro 2009; Chaplin 2009) (see Figure 19). Of specific interest, Timmermans et al. (2008) used the potential temperature and salinity measurements recorded by the six ITPs to estimate vertical heat fluxes via Kelley's (1990) laboratory-derived flux law. Figures 20 and 21 present the maps of average density ratio and associated heat flux as calculated in Timmermans et al. (2008).

Their study concluded that the vertical transport of heat from the AW is unlikely to have a significant impact

on the Arctic Ocean surface heat budget. Estimated vertical heat fluxes were found to be in the range 0.05-0.3 W/m^2, with the average value of 0.22 W/m^2; this is considerably less than the values derived from our 3D DNS results.

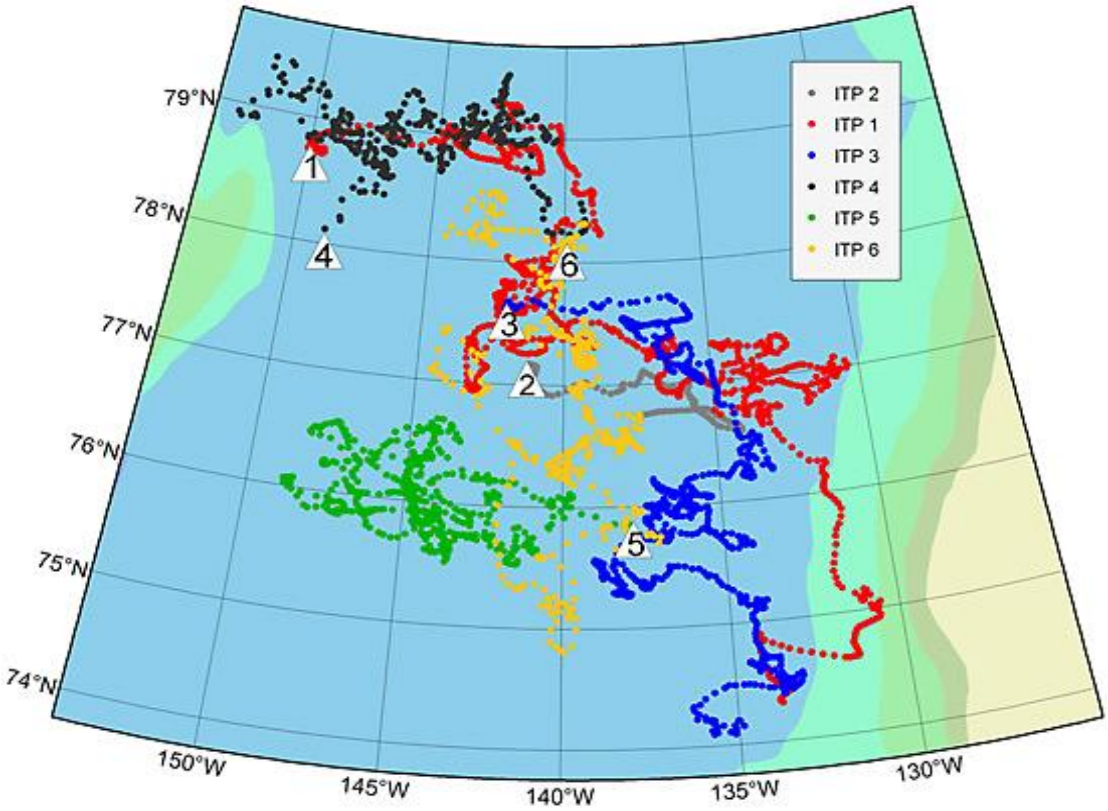

Figure 19. Trajectories of ITPs 1-6 (WHOI ITP website 2012).

By analyzing the same data as Timmermans et al. (2008) and applying the "new" flux law (22), a similar, but more up-to-date counterpart to Figure 21 can be obtained.

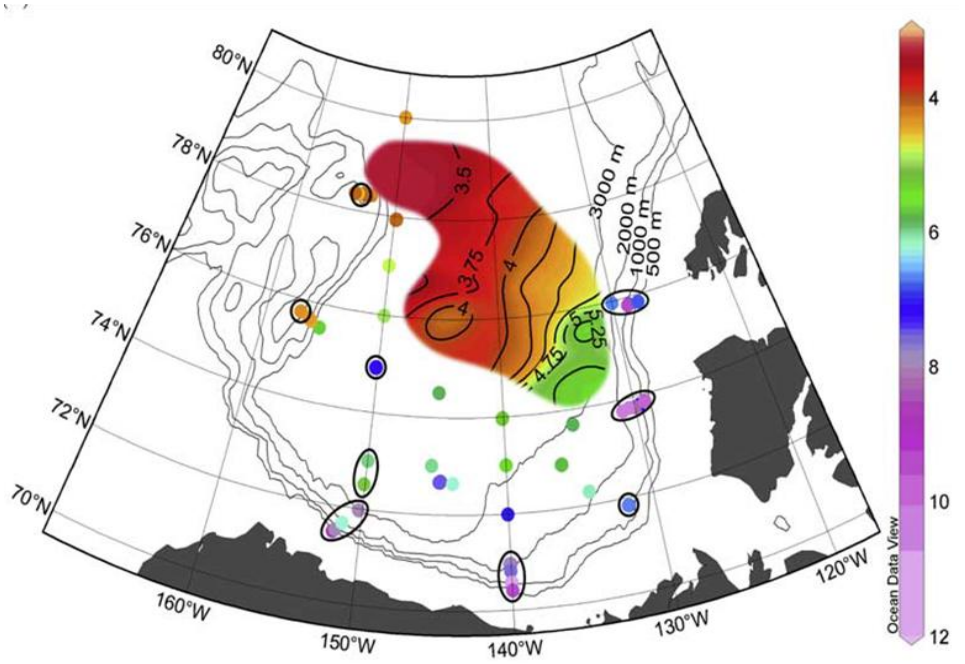

Figure 20. R_ρ averaged over the thermocline contoured from ITP measurements (After Timmermans et al. 2008).

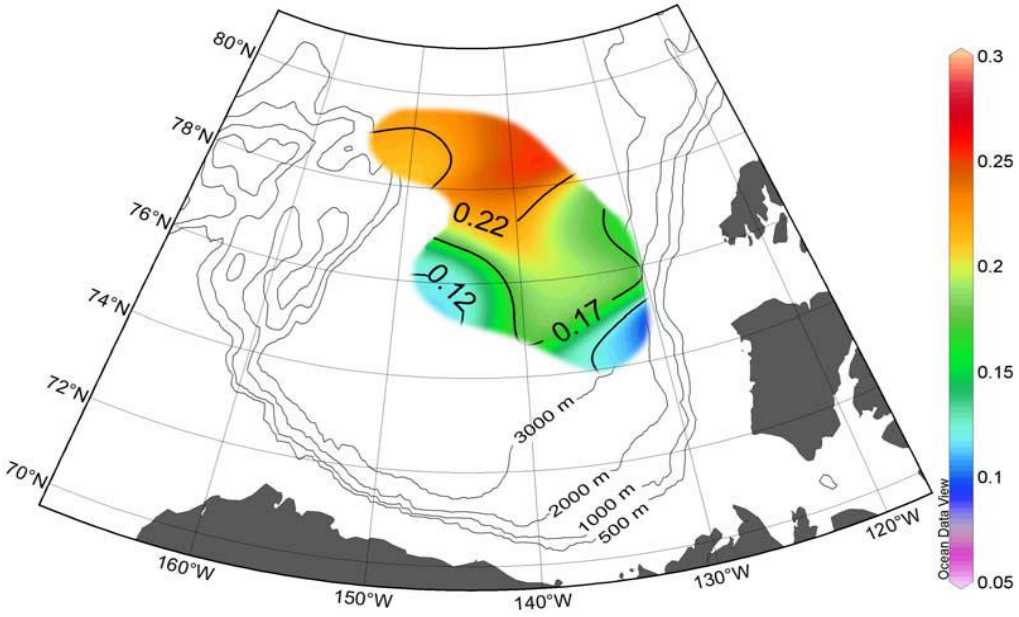

Figure 21. Map of heat flux (W/m^2) estimated by ITPs 1-6 profiles, averaged over the 200 m to 300 m deep thermohaline staircase (Timmermans et al. 2008).

B. DATA PROCESSING

The ITP data was arranged by profiler number 1-6 and processed together as one data set. Table 2 outlines the properties of these six ITPs. Processing began with the corrected ITP data obtained from the WHOI ITP website. Wilson (2007) suggested that anomalous results were obtained from the profiles corresponding to the downward data collection for each cast. Possibly due to sensor contamination, these measurements were affected, and all the downward collected profiles were removed from the total dataset. Figure 22 displays the location for each profile as well as the data-dense region chosen for analysis.

ITP	# of profiles	Duration	Distance	Launch Date	Recovery Date
1	2043	723	4990	8/15/05	8/8/07
2	244	40	378	8/19/04	9/28/04
3	1532	382	2559	8/23/05	9/9/06
4	698	349	2485	9/3/06	8/17/07
5	1095	450	3892	9/7/06	12/1/07
6	1335	1163	7353	9/4/06	10/11/09

Table 2. Properties of ITPs 1-6.

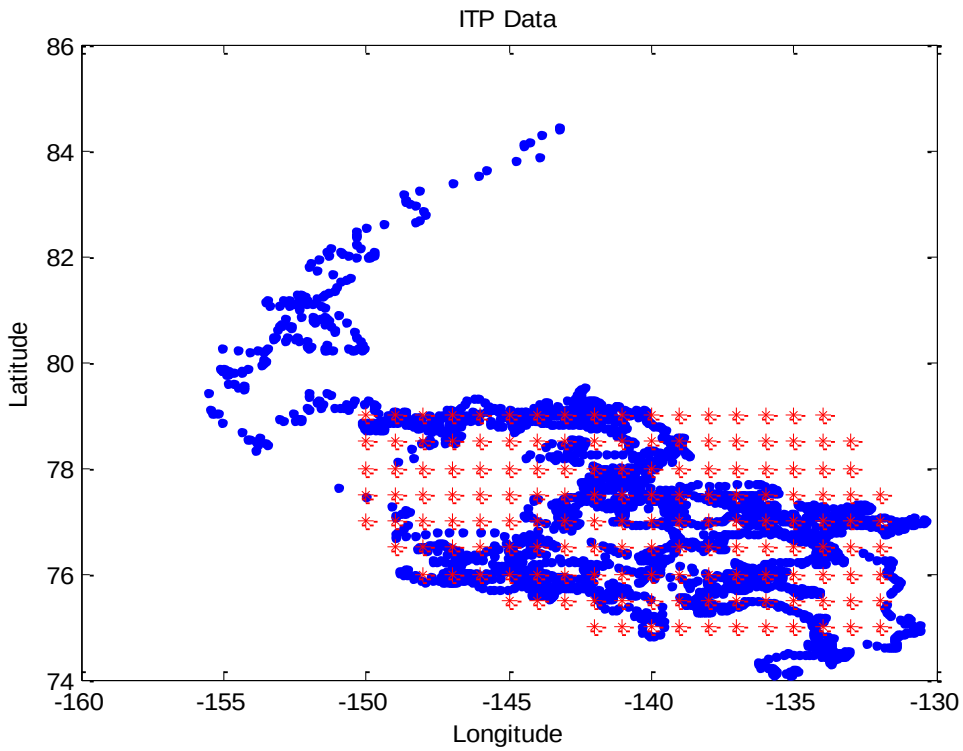

Figure 22. Locations for all ITP profiles. Red asterisks indicate the area analyzed in this study using the Matlab scattered data interpolation function.

The majority of diffusive layers occur in the 200-300 m region of the thermocline. The dataset was then reduced to only those data from 200-300 db pressures, which corresponds to roughly 195-295 m depth. By finding the local maximum value of potential temperature for each layer, the center of each layer was determined. Next the diffusive layers were classified independently of the particular cast using T-S plots. These plots (Figure 23) show vertical clusters at nearly constant salinity values that are indicative of horizontally homogeneous, diffusive layers. Due to the remarkable lateral coherence of layers in the thermohaline staircase, it was possible to

consolidate all six profilers' output into one dataset, by identifying the pronounced layers that appear uniformly throughout all the data (Chaplin 2009).

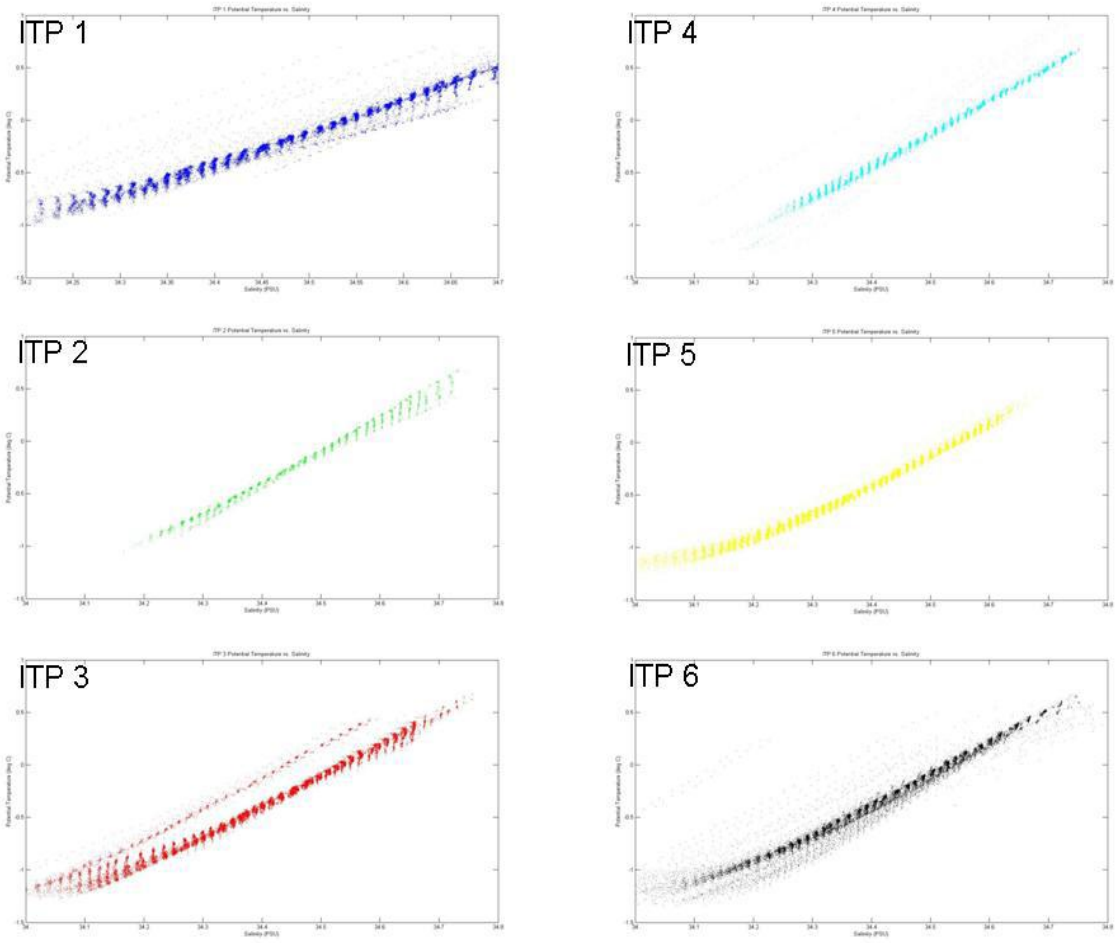

Figure 23. Temperature—Salinity plots for ITPs 1-6 (After Chaplin 2009).

This consolidation of data revealed a total of 19 vertical layers common to each profiler. Using the temperature and salinity jumps across each step, heat fluxes and density ratios were computed for each layer, and then vertically averaged over the entire thermocline.

C. RESULTS

Heat fluxes were derived using Kelley's (1990) flux law (8), and compared to those computed using Equation (22). Figure 24 is a contour map of $\bar{R}_\rho$ that can be used to quickly draw parallels between areas of low (high) density ratio and high (low) heat fluxes. Figures 25 and 26 are contour maps of heat flux colored using an identical scale for simple comparison between the two flux laws. Kelley's (1990) law used in Figure 25 under-predicts heat fluxes, on average, by a factor of two.

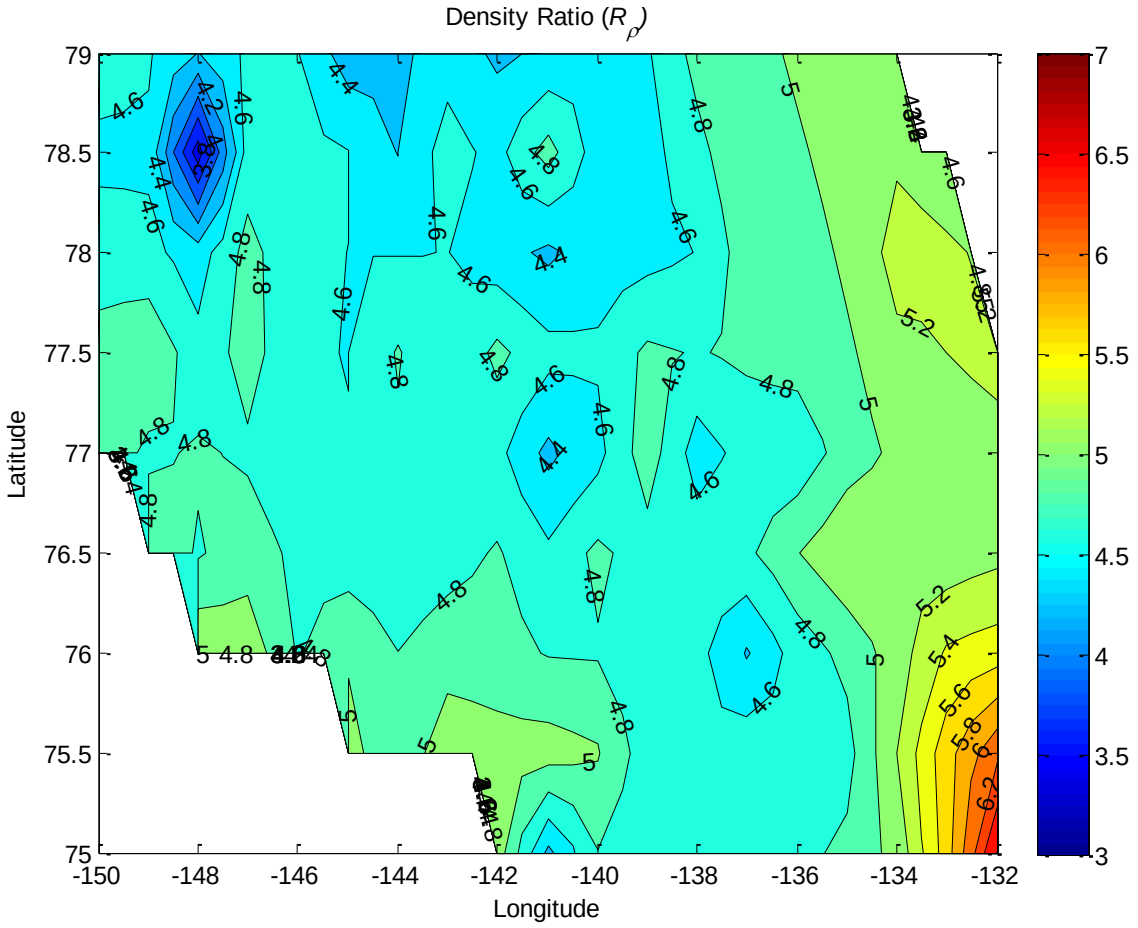

Figure 24. Contour map of $\bar{R}_\rho$ averaged over the 19 layers detected in the thermohaline staircase.

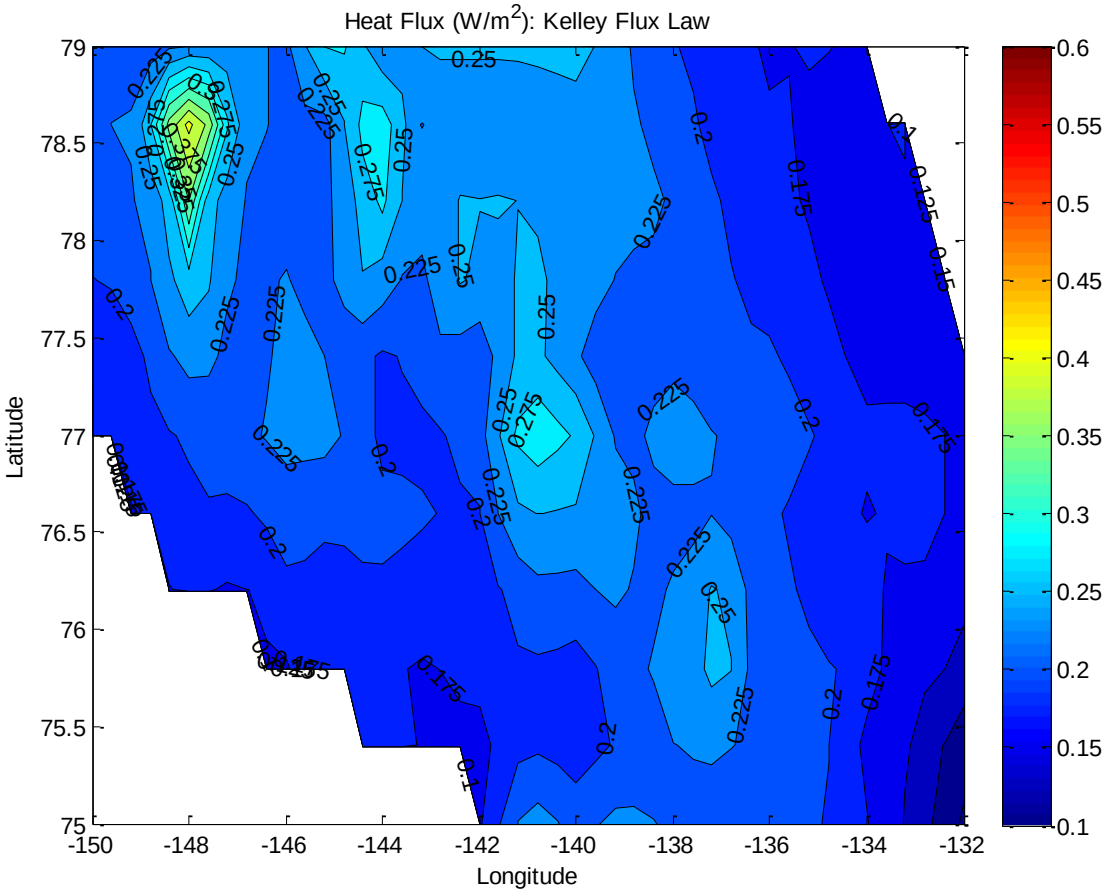

Figure 25. Contour map of heat flux (W/m^2) as computed by Kelley's (1990) four-thirds flux law, averaged over the 19 layers detected in the thermohaline staircase

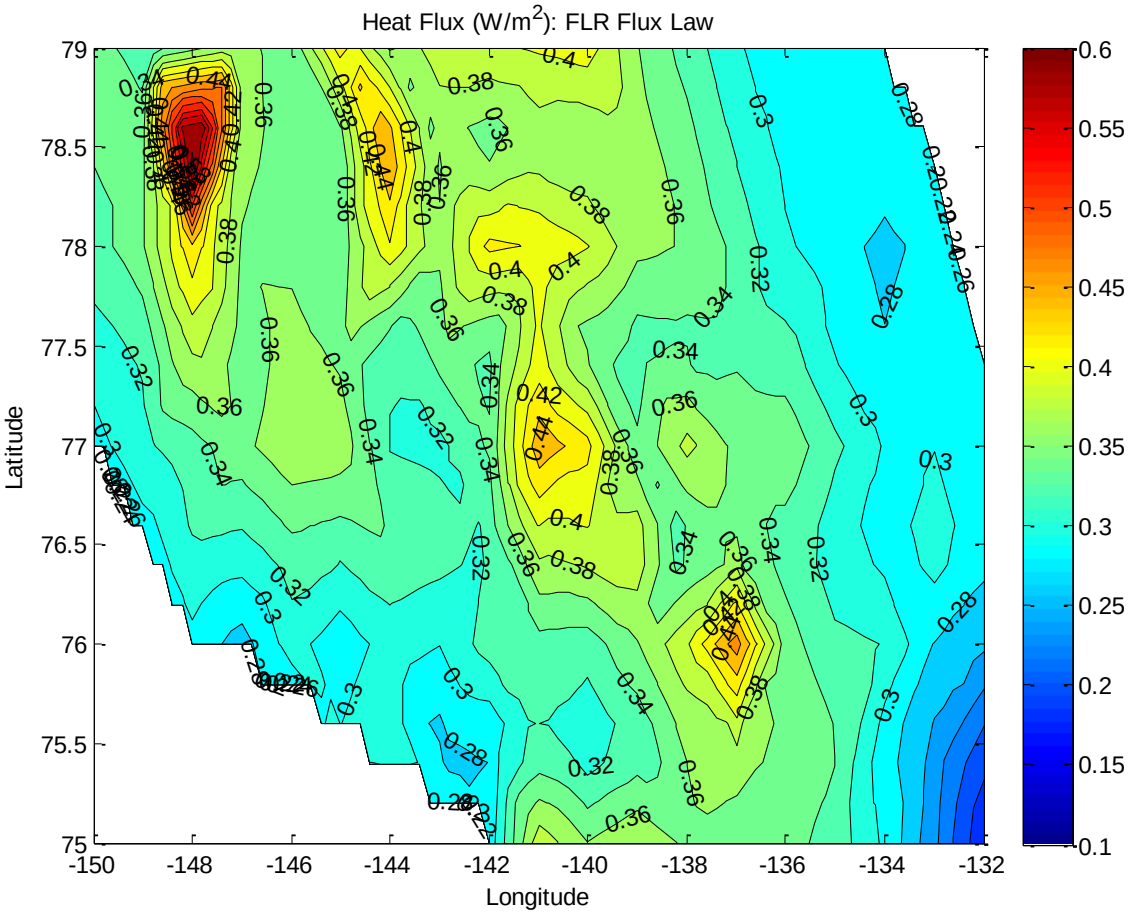

Figure 26. Contour map of heat flux (W/m^2) as computed by Equation (22), averaged over the 19 layers detected in the thermohaline staircase

V. CONCLUSIONS

A. DISCUSSION

3D DNS are proving to be the new standard for analysis of thermohaline staircases and the advective processes that transport heat upwards across diffusive interfaces. However, in order to provide reliable estimates of heat transport, simulations should meet a set of stringent requirements. In particular, simulations should

- Be performed at a resolution that adequately represents the scales of salt dissipation
- Utilize sufficiently large computational domains which replicate typical step-sizes in the Arctic staircase
- Be performed over a time period long enough to provide accurate statistical description
- Use parameters and conditions, such as a lack of rigid boundaries, reflective of those found in the Arctic thermocline

Such requirements are so computationally-demanding that, until now, DNS of Arctic staircases have been unfeasible. The fulfillment of such rigorous standards has allowed several important conclusions to be drawn.

It was determined that the extant laboratory-derived flux laws, while qualitatively consistent with numerical inferences, underestimate the vertical heat transport by as much as a factor of two. An alternative DNS-based flux law was formulated. The exponent of Turner's (1965) four-thirds flux law was also tested and found to not offer an optimal description of the numerical data. Evidence suggests that the 4/3 exponent in Equation (3) may require downward

adjustment by as much as 30%, if it is to be used for flux calculations.

Realistic 3D simulations which are inherently computationally expensive, were found to be consistent with the equivalent 2D DNS. The latter can provide an attractive alternative for sufficiently large density ratios ($R_\rho \geq 3$) but the margin of error increases with smaller density ratio values ($R_\rho < 2$).

The choice of boundary conditions (rigid versus periodic) and the experimental setup (run-down versus maintained) had a substantial effect on the vertical heat transport. It is suggested that oceanic staircases are better represented by models with maintained periodic boundary conditions.

Finally, Equation (22) was applied to ITP data in the vicinity of the Beaufort Gyre and the results compared with those from previous heat flux studies. It has been shown that the four-thirds flux law calculations underestimate heat flux by a factor of two across a range of density ratios representative of the Arctic thermocline, with $\overline{F}_H = 0.44$ W/m^2.

This study was prompted by the melting of Arctic sea-ice and the question as to whether double-diffusive convection can adequately shuttle AW water vertically to impact the melt rate of surface ice. Although the entire surplus of 1 W/m^2 of heat in the Arctic heat budget is not fully accounted for, our findings do help to close the gap. That vertical heat flux is (on average) twice as large as previously believed, points to diffusive convection playing a larger role in transporting AW vertically to the surface.

Alone or in combination, taking into account *all* ocean and atmospheric processes could explain the existing ice-melt observations and heat budget surplus. Furthermore, if AW continues to warm, double-diffusive convection will likely play a larger role in increasing the rate at which surface ice melts.

B. RECOMMENDATIONS

The analysis in this thesis warrants future work on the subject. Through further application of the DNS-derived flux law (22) to ITP data, the scope of study can be increased. For instance, the analysis of more recent data profiles can help determine the role of a continually-warming AW on the Arctic sea-ice melt rate. By taking a mean average, it would be relatively simple to determine the changes in vertical heat transport through Arctic thermohaline staircases over time.

Re-engaging in the inverse modeling technique that was started by Chaplin (2009) would also help to infer the vertical heat flux values through diffusive staircases. Previous findings support the DNS results from this study, but also raised questions on the algorithm performance and the sensitivities associated with the models due to varying layer thickness. These issues should be addressed in future research.

Finally, the newly derived flux parameterizations should be considered for inclusion into lower-resolution basin scale simulations in order to observe the impact of double diffusion on large-scale circulation patterns.

THIS PAGE INTENTIONALLY LEFT BLANK

LIST OF REFERENCES

Aagaard, K., and P. Greisman, 1975: Toward new mass and heat budgets for the Arctic Ocean. *Geophys. Res.*, **80**, 3821-3827.

Batchelor, G.K., 1953: *The Theory of Homogeneous Turbulence*. Cambridge University Press, 212 pp.

Canuto, C. G., M. Y. Hussaini, A.M. Quarteroni, and T.A. Zang. *Spectral Methods: Evolution to Complex Geometries and Applications to Fluid Dynamics*. Springer, 596 pp.

Caro, G. P., 2009: Direct numerical simulations of diffusive staircases in the Arctic. M.S. thesis, Dept. of Oceanography, Naval Postgraduate School, 61 pp.

Carpenter, J.R., T. Sommer, and A. Wuest, 2012: Simulations of a double-diffusive interface in the diffusive convection regime. *J. Fluid Mech.*, **711**, 411-436.

Chaplin, J. E., 2009: An inverse model of double diffusive convection in the Beaufort Sea. M.S. thesis, Dept. of Oceanography, Naval Postgraduate School, 89 pp.

Fetterer, F., K. Knowles, W. Meier, and M. Savoie, cited 2012: Sea Ice Index: Charctic Interactive Sea Ice Graph. Boulder, Colorado USA: National Snow and Ice Data Center. [Available online at http://nsidc.org/arcticseaicenews/charctic-interactive-sea-ice-graph/.]

Gardner, J., J. Richter-Menge, S. Farrell and J. Brozena, 2012: Coincident multiscale estimates of Arctic sea ice thickness. *Eos Trans. AGU*, **93(6)**, 57.

Huppert, H. E., 1971: On the stability of a series of double-diffusive layers. *Deep-Sea Res.*, **18**, 1005-1021.

Kelley, D. E., 1990: Fluxes through diffusive staircases: A new formulation. *J. Geophys. Res.*, **95**, 3365-3371.

Kelley, D. E., H. J. S. Fernando, A. E. Gargett, J. Tanny, and E. Ozsoy, 2003: The diffusive regime of double-diffusive convection. *Prog. Oceanogr.*, **56**, 461-481.

Krishfield, R. A., and D. K. Perovich, 2005: Spatial and temporal variability of oceanic heat flux to the Arctic ice pack. *J. Geophys. Res.*, **110**, C07021, doi:10.1029/2004JC002293.

Kolmogorov, A.N., 1941: The local structure of turbulence in incompressible viscous fluid over very large Reynolds numbers and Dissipation of energy in the locally isotropic turbulence. English Translations: *Proc. Roy. Soc. Phys.*, **A434**, 9–17.

Kwok, R., and N. Untersteiner, 2011: The thinning of Arctic sea ice. *Physics Today,* 36-41.

Marmorino, G. O., and D. R. Caldwell, 1976: Heat and salt transport through a diffusive thermohaline interface. *Deep Sea Res.*, **23**, 59-67.

Martinson, D. G., and M. Steele, 2001: Future of the Arctic Sea ice cover: Implications of an Antarctic analog. *Geophys. Res. Lett.*, **28**, 307–310.

Peyret, R., 2002: *Spectral Methods for Incompressible Viscous Flow*. Springer, 448 pp.

Perovich, D. K., T. C. Grenfell, J. A. Richter-Menge, B. Light, W. B. Tucker III, and H. Eicken, 2003: Thinner and thinner: Sea ice mass balance measurements during SHEBA, *J. Geophys. Res.*, **108(C3)**, 8050, 2003, doi:10.1029/2001JC001079.

Polyakov, I. V., and Coauthors, 2010: Arctic Ocean warming contributes to reduced polar ice cap. *J. Phys Oceanogr.*, **40**, 2743-2756, doi: 10.1175/2010JPO4339.1.

Prikasky, I.J., 2007: Direct numerical simulations of the diffusive convection and assessment of its impact on Arctic climate change. M.S. thesis, Dept. of Oceanography, Naval Postgraduate School, 81 pp.

Radko, T., and M. E. Stern, 1999: Salt fingers in three dimensions. *J. of Mar. Res.*, **57**, 471-502.

Radko, T., 2013: *Double-Diffusive Convection*. Cambridge University Press (In Print).

Rudels, B., L. G. Anderson, and E. P. Jones, 1996: Formation and evolution of the surface mixed layer and halocline of the Arctic Ocean. *J. Geophys. Res.*, **101**, 8807–8821.

Schmitt, R. W., 1994: Double diffusion in oceanography. *Annu. Rev. Fluid Mech.*, **26**, 255–285.

Steele, M., and T. Boyd, 1998: Retreat of the cold halocline layer in the Arctic Ocean. *J. Geophys. Res.*, **03**, 10 419–10 435.

Stellmach, S., and U. Hansen, 2008: An efficient spectral method for the simulation of dynamos in Cartesian geometry and its implementation on massively parallel computers. *Geochem. Geophys. Geosyst.*, **9(5)**, doi:10.1029/2007GC001778.

Timmermans, M. L., J. Toole, R. Krishfield, and P. Winsor, 2008: Ice-Tethered Profiler observations of the double-diffusive staircase in the Canada Basin thermocline. *J. Geophys. Res.*, **113**, doi:10.1029/2008JC004829.

Turner, J. S., 1965: The coupled transport of salt and heat across a sharp density interface. *Int. J. of Heat and Mass Transfer*, **8**, 759-767.

Turner, J. S., 1973: *Buoyancy Effects in Fluids*. Cambridge University Press, 367 pp.

Turner, J. S., 2010: The melting of ice in the Arctic Ocean: the influence of double-diffusive transport of heat from below. *J. Phys Oceanogr.*, **40**, 249-256.

Turner, J. S., and G. Veronis, 2004: The influence of double-diffusive processes on the milting of ice in the Arctic Ocean: Laboratory analogue experiments and their interpretation. *J. Mar. Syst.*, **45**, 21-37.

Wilson, A. L., 2007: Structure and dynamics of the thermohaline staircases in the Beaufort Gyre. M.S. thesis, Dept. of Oceanography, Naval Postgraduate School, 51 pp.

THIS PAGE INTENTIONALLY LEFT BLANK

INITIAL DISTRIBUTION LIST

1. Defense Technical Information Center
   Ft. Belvoir, Virginia

2. Dudley Knox Library
   Naval Postgraduate School
   Monterey, California

3. Dr. Peter Chu
   Naval Postgraduate School
   Monterey, California

4. Dr. Timour Radko
   Naval Postgraduate School
   Monterey, California

5. Dr. Jason Flanagan
   Naval Postgraduate School
   Monterey, California